JACS
JOURNAL OF THE AMERICAN CHEMICAL SOCIETY

Article

Rational Design of Mechanism-Based Inhibitors and Activity-Based Probes for the Identification of Retaining #-L-Arabinofuranosidases

Nicholas McGregor, Marta Artola, Alba Nin-Hill, Daniel Linzel, Mireille Haon, Jos Reijngoud, Arthur F. J. Ram, Marie-Noelle Rosso, Gijsbert A. van der Marel, Jeroen D. C. Codée, Gilles P. van Wezel, J-G Berrin, Carme Rovira, Herman S. Overkleeft, and Gideon J. Davies

J. Am. Chem. Soc., **Just Accepted Manuscript** • DOI: 10.1021/jacs.9b11351 • Publication Date (Web): 13 Feb 2020

Just Accepted

is published by the American Chemical Society. 1155 Sixteenth Street N.W., Washington, DC 20036

Rational Design of Mechanism-Based Inhibitors and Activity-Based Probes for the Identification of Retaining α-L-Arabinofuranosidases

Nicholas G.S. McGregor,[a,†] Marta Artola,[b,†] Alba Nin-Hill,[c,†] Daniël Linzel,[b] Mireille Haon,[d] Jos Reijngoud,[e] Arthur Ram,[e] Marie-Noëlle Rosso,[d] Gijsbert A. van der Marel,[b] Jeroen D.C. Codée,[b] Gilles P. van Wezel,[e] Jean-Guy Berrin,[d] Carme Rovira,*[,c,f] Herman S. Overkleeft,*[,b] Gideon J. Davies*[,a]

[a]York Structural Biology Laboratory, Department of Chemistry, The University of York, Heslington, York, YO10 5DD [b]Leiden Institute of Chemistry, Leiden University, Einsteinweg 55, 2300 RA Leiden, The Netherlands, [c]Departament de Química Inorgànica i Orgànica (Secció de Química Orgànica) & Institut de Química Teòrica i Computacional (IQTCUB), Universitat de Barcelona, Martí i Franquès 1, 08028 Barcelona, Spain, [d]INRA, Aix Marseille University, Biodiversité et Biotechnologie Fongiques (BBF), UMR1163, F-13009 Marseille, France. [e]Molecular Microbiology and Biotechnology, Institute of Biology Leiden, Leiden University, Sylviusweg 72, 2333 BE Leiden, The Netherlands, [f]Institució Catalana de Recerca i Estudis Avançats (ICREA), 08020 Barcelona, Spain.

[†]These authors contributed equally to this work.

* Corresponding authors

KEYWORDS: Activity-based protein profiling, cyclophellitol, secretome, glycoside hydrolase, α-L-arabinofuranose

ABSTRACT: Identifying and characterizing the enzymes responsible for an observed activity within a complex eukaryotic catabolic system remains one of the most significant challenges in the study of biomass-degrading systems. The debranching of both complex hemicellulosic and pectinaceous polysaccharides requires the production of α-L-arabinofuranosidases among a wide variety of co-expressed carbohydrate-active enzymes. To selectively detect and identify α-L-arabinofuranosidases produced by fungi grown on complex biomass, potential covalent inhibitors and probes which mimic α-L-arabinofuranosides were sought. The conformational free energy landscapes of free α-L-arabinofuranose and several rationally designed covalent α-L-arabinofuranosidase inhibitors were analyzed. A synthetic route to these inhibitors was subsequently developed based on a key Wittig-Still rearrangement. Through a combination of kinetic measurements, intact mass spectrometry, and structural experiments, the designed inhibitors were shown to efficiently label the catalytic nucleophiles of retaining GH51 and GH54 α-L-arabinofuranosidases. Activity-based probes elaborated from an inhibitor with an aziridine warhead were applied to the identification and characterization of α-L-arabinofuranosidases within the secretome of *A. niger* grown on arabinan. This method was extended to the detection and identification of α-L-arabinofuranosidases produced by eight biomass-degrading basidiomycete fungi grown on complex biomass. The broad applicability of the cyclophellitol-derived activity-based probes and inhibitors presented here make them a valuable new tool in the characterization of complex eukaryotic carbohydrate-degrading systems and in the high-throughput discovery of α-L-arabinofuranosidases.

INTRODUCTION

Carbohydrate-degrading machinery is a fundamentally important component of the metabolic systems that underpin the global carbon cycle. Our understanding of these systems is dependent on an ability to identify the capacities of the carbohydrate-active enzymes produced by an organism. The growth of genomic libraries has revealed an expansive world of carbohydrate-degrading enzymes, of which only a small fraction have been isolated and probed for catalytic potential.[1] Transcriptomic and proteomic experiments comparing the gene expression and protein secretion patterns of organisms grown on different substrates have helped to identify the genetic logic used by these organisms to efficiently degrade recalcitrant biomass.[2] However, the underlying chemical rationale for these expression patterns remains obscure without highly detailed experimental work characterizing the role of each enzyme.

Inspired by the work of Withers[3–5] and Wright[6], we have been developing cyclophellitol-derived activity-based inhibitors and probes (some aspects of which are reviewed in [7–9]) for the rapid detection and identification of specific biomass-degrading glycoside hydrolases within complex systems. The potential of cyclophellitol-derived activity-based probes (ABPs) as tools for the detection and identification of retaining glycoside hydrolases has been well-established.[10] Mimicking the half chair conformation of the enzymatic transition state, cyclophellitol and cyclophellitol aziridine derivatives react specifically with the catalytic nucleophile of a retaining glycoside hydrolase, forming a non-hydrolyzable ester linkage through a ring-opening addition.[11] This general strategy has been exploited to inhibit and label glycosidases displaying a variety of specificities including α- and β-D-glucosidases[12–14], β-D-glucuronidases[15], and α- and β-D-galactosidases[16,17] among others. Building on this work, we have recently

reported the synthesis and validation of a collection of cyclophellitol-derived inhibitors and probes which specifically label retaining β-D-xylanases and β-D-xylosidases.[18] These compounds were able to efficiently attach chemical handles for the detection and identification of key secreted xylan-degrading enzymes within an *Aspergillus* secretome. Expanding this toolbox to target side-chain removal enzymes has remained a challenge, not least for furanoside-active enzymes.

α-L-Arabinofuranoside "side-chains" are commonly found on both hemicellulosic and pectinaceous plant polysaccharides. The efficient removal of α-L-arabinofuranose branches enhances the breakdown of xylan-rich biomass.[19] Furthermore, α-L-arabinofuranosidases are an essential part of the polysaccharide utilization loci which ferment arabinan chains in dietary rhamnogalacturonan I and arabinogalactan within the human gut.[20] Thus, cyclophellitol-derived ABPs and inhibitors for α-L-arabinofuranosidases could be used to identify the enzymes responsible for the breakdown of a variety of complex polysaccharides. However, it is not currently known whether cyclophellitol derivatives can be effectively extended to target furanosidases.

No route to the synthesis of covalent inhibitors of α-L-arabinofuranosidases has previously been identified. The first synthesis of covalent furanose-configured inhibitors was the preparation of β-D-arabinofuranosyl and α-L-xylofuranosyl aziridines reported by Bols *et al.* in 2003.[21] These were prepared via N-O reduction of cyclopentaisoxazolidines. Due to the inverted stereochemistry of the electrophilic moiety with respect to C4 (carbohydrate numbering), this synthetic strategy cannot be translated to α-L-arabinofuranose analogues, so new synthetic methodologies are needed to expand the scope of synthetically accessible furanoside mimics.

We have designed a collection of putative α-L-arabinofuranosidase inhibitors and ABPs with different electrophilic traps and detection tags. Potential inhibitors were analyzed *in silico* for their ability to mimic the natural 5-membered ring structure, stereochemistry, and conformational itinerary of retaining α-L-arabinofuranosides. These inhibitors and probes were synthesized following a general route inspired by the synthesis of six-membered cyclophellitol derivatives. Inhibition kinetics measured with α-L-arabinofuranosidases from glycoside hydrolase families 51 and 54 (GH51 and GH54), the two major families of retaining α-L-arabinofuranosidases, were measured to validate our predictions. Furthermore, the ability of our α-L-arabinofuranosidase probes to facilitate the selective detection, identification, and characterization of active GH51 and GH54 enzymes within the complex mixture of enzymes secreted by *Aspergillus niger* was validated. These methods were then extended to the identification of α-L-arabinofuranosidases within the secretomes of basidiomycete fungi grown on complex biomass.

EXPERIMENTAL

All chemicals were purchased from Sigma-Aldrich unless otherwise specified.

Design and synthesis of α-L-arabinofuranose-configured cyclophellitol derivatives

Detailed protocols for synthesis of compounds **1** to **23** and their NMR characterization can be found in the supplementary materials.

Secretome production

Aspergillus niger strain N402 was grown as described by Schröder et al.[18] with a mixture of 50 mM arabinose, 1% sugar beet arabinan, and 2 mM fructose as the sole carbon source. Samples were collected, 0.2 μm-filtered, and snap-frozen after 5 days. Samples were stored at -80°C until being thawed immediately before use.

The strains *Abortiporus biennis* BRFM 1215 (*A. biennis*), *Fomes fomentarius* BRFM 1323 (*F. fomentarius*), *Hexagonia nitida* BRFM 1328 (*H. nitida*), *Leiotrametes menziesii* BRFM 1557 (*L. menziesii*), *Polyporus brumalis* BRFM 958 (*P. brumalis*), *Trametes ljubarskyi* BRFM 957 (*T. ljubarskyi*) *Trametes gibbosa* BRFM 952 (*T. gibbosa*), and *Trametes meyenii* BRFM 1361 (*T. meyenii*) were obtained from the CIRM-CF collection (International Centre of Microbial Resources dedicated to Filamentous Fungi, INRA, Marseille, France). All strains were identified by morphological and molecular analysis of ITS (Internal Transcribed Spacer) sequences. The strains were maintained on malt agar slants at 4°C.

Basidiomycete cultures were grown in 250 mL baffled Erlenmeyer flasks with 100 mL medium containing 2.5 g L^{-1} of maltose as a starter (except for the maltose control condition; 20 g L^{-1}), 1.842 g L^{-1} of diammonium tartrate as a nitrogen source, 0.5 g L^{-1} yeast extract, 0.2 g L^{-1} KH_2PO_4, 0.0132 g L^{-1} $CaCl_2/2H_2O$ and 0.5 g L^{-1} $MgSO_4/7H_2O$, and as a main carbon source, 15 g L^{-1} (dry weight) of wheat straw (*Triticum aestivum*) or Wiley-milled aspen (*Populus grandidentata*). Cultures were incubated in the dark at 30°C with shaking at 120 rpm. The cultures were stopped 10 days after inoculation and the culture broths (secretomes) were filtered using 0.2 μm polyethersulfone membrane (Millipore) and then stored at -20°C until use.

Recombinant enzyme production

The coding sequence for *Geobacillus stearothermophilus* abfA (GsGH51, GenBank: AAD45520) was synthesized with *E. coli* codon optimization and cloned into pET28a(+) with an N-terminal TEV protease-cleavable 6xhis tag by GenScript. Following transformation of BL21(DE3) Gold, the enzyme was produced in an auto induction medium (1% tryptone, 0.5% yeast extract, 25 mM Na_2HPO_4, 25 mM KH_2PO_4, 50 mM NH_4Cl, 5 mM Na_2SO_4, 0.05% glucose, 0.5% glycerol, 0.2% lactose) at 37°C. The enzyme was purified as described previously[22] with an added overnight treatment with his-tagged TEV protease S219V[23] in pH 8 Tris-HCl, 5 mM DTT, 1 mM EDTA at RT followed by inverse histrap purification and desalting into 5 mM Tris-HCl, 1 mM EDTA, pH 8.0.

Aspergillus niger abfA (AnAbfA, GenBank: CAK43424) and *Aspergillus kawachii* abfB (AkAbfB, GenBank: BAB96816) were produced in *P. pastoris* X-33. A plasmid encoding AkAbfB in pPICZα with no purification tag was obtained from professors Takuya Koseki and Shinya Fushinobu. AnAbfA was synthesized by IDT as a GBlock and cloned into the vector fragment PCR-amplified from the AkAbfB-pPICZa plasmid using Gibson assembly[24]. The AkAbfB (E221Q) mutant was generated using the Q5 site-directed mutagenesis kit (New England Biolabs) with primers designed by the NEBaseChanger tool.

Plasmid DNA for transformation into *P. pastoris* was linearized with SacI and purified using a PCR clean-up kit (Qiagen) using

ultrapure water as the eluent. 100 ng of linearized DNA was electroporated into 80 µL of X-33 electrocompetent cells prepared following the protocol of Wu and Letchworth.[25] Nine colonies from each transformation were purified on YPD-Zeocin plates, then grown in 5 mL of BMGY medium. At saturation (OD600 ~ 20) cells were collected by centrifugation and re-suspended in 5 mL of BMMY medium for expression screening at 20°C. The transformant which gave the highest titer of the target protein with minimal detectable contamination after 3 daily 0.5% MeOH feedings was grown in 500 mL of BMGY in a 2.5 L baffled shaking flask at 30°C overnight. The culture was then cooled to 20°C and supplemented with 2.5 mL of 100% MeOH each day for 3 days.

The culture supernatant was clarified by centrifugation followed by 0.45 µm-filtration. 500 mL of medium was concentrated using a KrosFlo tangential flow system fitted with a 30 kDa MWCO mPES filter, then diluted with 9 volumes of 10 mM pH 5 sodium acetate buffer and concentrated again. Protein was then collected onto a 5 mL Q sepharose HP column (GE Healthcare), washed with 3 CV of 50 mM pH 5 sodium acetate buffer, then eluted with a 25 CV gradient from 0 to 0.5 M NaCl in the same buffer. Fractions from the largest UV-active peak were pooled, concentrated to 10-30 mg/mL using a 30 kDa MWCO centrifugal concentrator (Amicon) and purified over Superdex 200 (GE Healthcare) into 50 mM sodium acetate pH 5. Protein-containing fractions were pooled and concentrated to give a colorless 15-25 mg/mL protein solution. ~5 mg of protein was then treated with 1000 U of EndoHf (New England Biolabs) overnight at RT. This was purified using a 5 mL Q sepharose HP column as above. To prepare the sample for crystallization, the eluent from Q sepharose was mixed 1:1 with saturated ammonium sulfate and purified over a 1 mL phenyl sepharose HP column with a 25 CV gradient from 2 M ammonium sulfate to 0 M ammonium sulfate in 50 mM pH 5 sodium acetate buffer. Protein-containing fractions were pooled, desalted into 20 mM sodium acetate pH 5, concentrated to 10-30 mg/mL and frozen at -80°C.

Enzyme visualization with ABP 4

ABP **4** was dissolved in DMSO to prepare a 10 mM stock solution which was diluted in ultrapure water. Unless otherwise noted, samples were stained with 10 µM ABP **4** at 37°C for 30 minutes at pH 6.5 and proteins were separated at 200 V using either a precast 4-20% (Bio-Rad) or an 8.75% 1 mm miniprotean SDS-PAGE gel. Fluorescence was imaged using a Typhoon 5 laser scanner with the Cy5 laser and filter set. Enzyme molecular weights were estimated using a Pageruler 10-180 kDa pre-stained protein ladder.

Basidiomycete secretomes were buffered with 0.1 volumes of 1 M NH_4OAc pH 5.5. For screening, 17.2 µL of buffered secretome was mixed with 2.8 µL of 60 µM ABP **4** and incubated for 1 hour at 30°C. The sample was then supplemented with 2 µL of 10X glycoprotein denaturing buffer (New England Biolabs), heated to 95°C for 5 minutes and split in half. Each half was mixed with 10 µL of 2x PNGaseF mastermix (2X glycobuffer 2, 2% NP-40 containing either 0 or 7.5 U/µL of PNGaseF) and incubated for 1 hour at 37°C. Samples were then diluted with 6.7 µL of 4X SDS-PAGE loading dye, heated to 95°C for 5 minutes and 10 µL was separated through a 4-15% Criterion (Bio-Rad) gel.

For scaled up labelling, 20 µL of 60 µM ABP **4** was added to 100 µL of buffered secretome and incubated at 30°C for 1 hour. 500 µL of acetone was then added and the samples were incubated at -20°C for 1 hour. Precipitate was collected by centrifugation at 10000 x *g* for 5 minutes at 4°C. The supernatant was discarded, and the sample was left to air dry to minimize residual acetone. The sample was then re-suspended in 20 µL of 1X SDS-PAGE loading dye and heated to 95°C for 5 minutes to dissolve. The entire sample was then separated through a 4-20% gel.

In situ characterization of secreted enzymes

The pH optimum of enzyme labelling was determined by visualization with ABP **4** using the standard protocol (above) with variable buffer solutions including a series of McIlvane buffers prepared at 0.5 M strength (0.28 M citrate, 0.22 M phosphate) from pH 2-7.5 in 0.5 pH unit increments and a series of succinate-phosphate-glycine (SPG) buffers prepared at 0.5 M strength (62.5 mM succinic acid, 219 mM phosphate, 219 mM glycine) from pH 4-10 in 1 pH unit increments. 5 µL of each buffer was added to 45 µL of *A. niger* arabinan secretome immediately prior to ABP addition.

The thermal tolerance of secreted enzymes was assayed at the inhibition optimum (50 mM pH 6.5 phosphate buffer) by incubating the *A. niger* arabinan secretome at temperatures ranging from RT to 95°C for 1 hour. Secretome samples were then rapidly cooled to 20°C and enzymes were visualized with ABP **4** using the standard protocol.

Measuring irreversible inhibition kinetics

The kinetics of enzyme inhibition were measured using a continuous assay[26,27] at 25°C in a 384-well plate with 4-methylumbelliferyl α-L-arabinofuranoside (4MU-Araf) as substrate. Kinetic measurements were made in technical quadruplicate. Curve fitting and statistical analysis was performed using OriginPro graphing software. Enzymes were diluted in 50 mM sodium phosphate buffer pH 7.0. Substrate was dissolved in DMSO to give a 100 mM stock which was diluted with ultrapure water. Putative inhibitors were dissolved in and diluted with ultrapure water with the exception of inhibitor **3** which was dissolved in DMSO to give a 50 mM stock, which was diluted with ultrapure water.

Enzyme specific activity was initially assessed by monitoring the hydrolysis of 50 µM 4MU-Araf in pH 7 phosphate for 10 minutes. Michaelis-Menten parameters for the hydrolysis of 4MU-Araf were estimated by varying the substrate concentration from 4 to 500 µM and fitting a site-saturation kinetic model ($v_0/[E]_t = k_{cat}[S]_0/K_M+[S]_0$) to the resulting rate vs. substrate concentration data (Supplemental Table 1, Supplemental Figure 1A, Supplemental Figure 2A). Measurements were made at an excitation wavelength of 390 nm (15 nm bandwidth) to eliminate primary inner filter effects at substrate concentrations as high as 500 µM in our assay format (Supplemental Figure 3). Inhibition kinetics were measured using a substrate concentra-

tion of 100 μM and an excitation wavelength of 360 nm, an enzyme concentration of 50 ng/mL, and variable inhibitor concentrations. Each fluorescence vs. time curve was fitted with an exponential decay model ($F = F_\infty(1-e^{-k_{app}t})$). The resulting apparent decay constants were plotted against inhibitor concentration and fitted with a site-saturation kinetic model with correction for competition by the substrate using the measured K_M value and the initial substrate concentration ($k_{app} = k_{inact}[I]_0/1+([S]_0/K_M)+([I]_0/K_I)$).

Intact MS following enzyme labelling

GsGH51 or EndoH-treated AkAbfB were diluted to 0.1 mg/mL in their respective SEC elution buffers. Compounds **1**, **2,** or **6** were added to a final concentration of 50 μM and incubated for 30 minutes at RT. The treated protein samples were diluted with 4 volumes of 1% formic acid, 10% acetonitrile and 5 μL was injected over an MSPac DS-10 Desalting Cartridge flowing at 30 μL/min using a NanoAcquity HPLC (Waters). Following a 5-minute wash with 20% acetonitrile, 0.1% formic acid in water, protein was eluted into a maXis UHR-Tof (Bruker) with a 10-minute gradient from 20-55% acetonitrile. The column was washed for 2 minutes with 80% acetonitrile and equilibrated for 3 minutes with 20% acetonitrile between runs. Following protein signal integration and baseline subtraction, spectra were deconvoluted using the maximum entropy algorithm within COMPASS to calculate protein mass.

Enzyme pull-down using ABP 5

A. niger arabinan secretome was buffered with 50 mM McIlvane buffer pH 6.5, then treated with 0.1 mM inhibitor **2** or DMSO control for 1 hour at 37°C (inhibitor **6** is also suitable for pre-treatment, Supplemental Figure 4). Following this, the secretome was treated with either 20 μM ABP **5** or DMSO control for 30 minutes at 37°C. Biotinylated proteins were pulled down, digested, and identified as described by Schröder *et al.*[18] Basidiomycete secretome samples were processed without concentration or lyophilization with three modifications to the protocol: firstly, protein was precipitated through the addition of 4 volumes of acetone followed by incubation at -20°C for 1 hour; secondly, following the initial strep mag sepharose bead wash with 0.5% SDS, beads were washed with 2% SDS at 65°C for 10 minute with agitation followed by 2 M urea and then PBS; and lastly, peptides liberated through on-bead digest were modified with TMT0 following the manufacturer's instructions prior to LC-MS/MS analysis using an Orbitrap Fusion Tribrid mass spectrometer (Thermo Scientific). Peptides were identified by mapping onto the predicted proteomes deduced from genome sequence of *A. biennis* BRFM 1778, *F. fomentarius* BRFM 1823, *L. menziesii* BRFM 1781, and *T. gibbosa* BRFM 1770. For each genome (to be published elsewhere), CAZymes were annotated as in Lombard *et al.*, 2014[1]. All genome and proteome data are publicly available on the Mycocosm portal (www.mycocosm.jgi.doe.gov).

Enzyme crystallization and diffraction

Crystals of GsGH51 were grown essentially as described by Hövel *et al.*[22] Optimized crystals were grown by mixing 1.2 μL of protein (10 mg/mL in 5 mM Tris-HCl pH 8.0) with 0.6 μL of well solution containing 15% PEG3350, 5% 2-propanol, 0.1 M Tris-HCl pH 7.5, 0.80 M NH_4F in a sitting drop at 293 K (Supplemental Figure 5A). To generate inhibitor-bound complexes, crystal-containing droplets were supplemented with 0.1 μL of 2 mM inhibitor in water and incubated overnight prior to cryo-protection in well solution supplemented with 12.5% glycerol and flash freezing in LN_2.

Initially, crystals of AkAbfB were grown essentially as described by Miyanaga *et al.*[28] Optimized crystals grew from 0.5 μL of 10 mg/mL AkAbfB in 50 mM pH 5 sodium acetate mixed with 0.5 μL of 100 mM Tris-HCl pH 8.0, 200 mM $MgCl_2$, 400 mM NaCl, 20% PEG6000, 2.5% DMF at 279 K. However, preferential formation of poor-quality needle clusters and poor diffraction of these crystals led us to explore other crystallization conditions. EndoH-deglycosylated AkAbfB or AkAbfB (E221Q) (12 mg/mL in 50 mM sodium acetate pH 5.0) formed slow-growing isolated crystals when mixed 2:1 with 0.2 M lithium sulfate, 0.1 M sodium acetate pH 4.5, 50% PEG400 (Supplemental Figure 5B). Supplementation with 0.2-0.5 M NaCl resulted in more rapid crystal growth. To generate inhibitor-bound complexes, crystals were transferred to mother liquor supplemented with inhibitor **6** or **2** to a final concentration of 0.2 mM**,** or saturated with PNP-Araf (for AkAbfB (E221Q)). Crystals were soaked for 1 hour at RT prior to freezing.

Diffraction data were collected at Diamond Light Source (Harwell, UK) on beamline I04 and automatically processed using the fast_dp[29] (GsGH51), autoPROC[30] (AkAbfB-**2** and AkAbfB-**6**), or Xia2[31] (AkAbfB-PNP-Araf) pipelines. Computation was carried out using programs from the CCP4 suite[32] unless otherwise stated. All crystal structure figures were generated using Pymol (Schrodinger). Data collection and processing statistics for all structures are given in Supplemental Table 2.

Structure solution and refinement

Data for GsGH51 bound to inhibitors **2** and **6** were collected to 1.40 Å. Each structure was solved by molecular replacement using Phaser[33] with the known structure (PDBID: 1pz3) as the search model. The resulting solution showed clear density for the bound ligand within the enzyme active site. Ligand coordinates and dictionaries were generated using jLigand[34] and built into the model using Coot[35], followed by alternating rounds of manual model building and refinement using Coot and REFMAC5[36].

Data for AkAbfB bound to inhibitors **2** and **6** were collected to 1.47 and 1.86 Å, respectively. Each structure was solved by molecular replacement using Phaser with the known structure (PDBID: 1wd3) as the search model. The resulting solution showed clear density for the bound ligand within the enzyme active site. The structures were refined, as above, and the same ligand coordinates and geometries were used.

Data for AkAbfB (E221Q) bound to PNP-Araf were collected to 1.64 Å. The structure was solved by molecular replacement using Phaser with the AkAbfB-**2** complex as the search model. The resulting structure showed clear density for two PNP-Araf (ligand ID: KHP) molecules bound to the carbohydrate-binding module. Following several rounds of manual model building and refinement, partial density for an additional PNP-Araf molecule, which was modelled at 60% occupancy, became apparent in the active site.

Conformational analysis

Conformational free energy landscapes (FELs) were computed for α-L-arabinofuranose and compounds **1**, **2**, and **6** using Density Functional Theory-based molecular dynamics (MD), according to the Car-Parrinello (CP) method.[37] Each molecule was enclosed in an isolated cubic box of 12.5 Å × 12.5 Å × 12.5 Å. A fictitious electron mass of 500 atomic units (a.u.) was used for the CP Lagrangian and a time step of 0.12 fs was used in all CPMD simulations to ensure that the adiabacity of the fictitious kinetic energy of the electrons was smaller than 10^{-5} a.u./atom. The Kohn-Sham orbitals were expanded in a plane wave basis set with a kinetic energy cut-off of 70 Ry. *Ab initio* pseudopotentials, generated within the Troullier-Martins scheme, were employed.[38] The Perdew, Burke, and Ernzerhoff generalized gradient-corrected approximation[39] was selected in view of its good performance[40] in previous work on isolated sugars[41], glycosidases, and glycosyltransferases[42]. The metadynamics algorithm[43], provided by the Plumed 2 plugin[44], was used to explore the conformational free energy landscape of the systems, taking as collective variables the pseudorotational phase (φ) puckering coordinate[45,46], as well as a dihedral angle accounting for the rotation of the sugar hydroxymethyl group. The energy was projected into the φ coordinate for representation purposes. Initially, the height of these Gaussian terms was set at 0.6 kcal/mol and a new Gaussian-like potential was added every 500 MD steps. Once the whole free energy space was explored, the height of the Gaussian terms was reduced to 0.2 kcal/mol to facilitate convergence of the FEL. The width of the collective variables was set according to their oscillations in the free dynamics which corresponded to 0.035 and 0.1 rad for φ and the hydroxymethyl dihedral angle, respectively. The simulations were stopped when energy differences among wells remain constant, which was further confirmed by a time-independent free energy estimator.[47] The exploration of the phase space was extended up to 380, 360, 324, and 474 ps for α-L-arabinofuranose, compound **1**, compound **2**, and compound **6**, respectively. The errors in the principal minima, taken as a standard deviation (SD) from the last 200 ps, are below 0.6 kcal mol^{-1}. Conformational FELs computed using only φ as CV gave very similar results.

The Michaelis complexes of compounds **1**, **2**, and **6** were modelled using the crystal structures of the adducts obtained for GsGH51 and AkAbfB as a reference. In the case of compounds **1** and **2**, the Michaelis complex was reconstructed by removing the covalent bond between the inhibitor and the nucleophile in the protein structure bound to inhibitor **2**. The amine group was reverted to an aziridine (compound **2**), which was replaced with an oxygen atom to give compound **1**.

Molecular dynamics (MD) simulations were set up employing the program LEaP included in the Amber suite[48] and the ff14SB protein force field[49]. The compounds were parametrized using gaff2[50]. The systems were solvated with explicit TIP3P water molecules.[51] They were neutralized with 31 and 21 sodium atoms for all neutral compounds in GsGH51 and AkAbfB, respectively. The systems with protonated compound **2** were neutralized with one fewer sodium atom (30 and 20 in GsGH51 and AkAbfB, respectively). MD simulations were performed using Amber16[48]. A thermal equilibration to 300 K was done prior to the equilibration of dynamics in the NPT ensemble with a production phase of 51 ns for each system. The SHAKE algorithm, with an integration time step of 2 fs, was used. The binding free energy of the compounds were obtained by using the MMPBSA

method[52] integrated in the Amber suite.

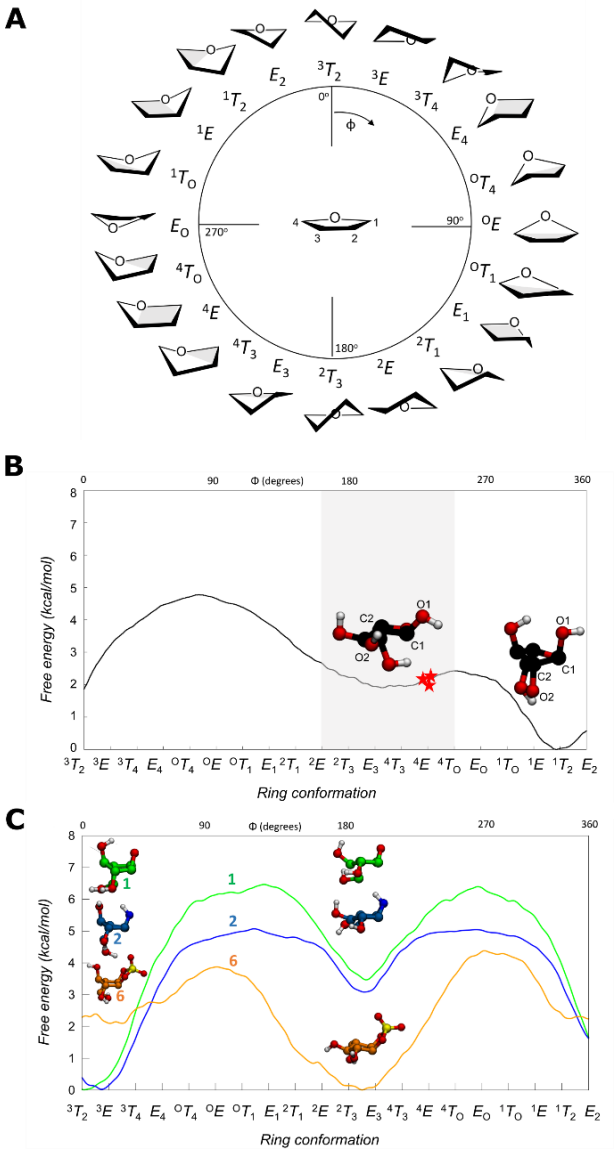

Figure 1. A) Graphical representation of the conformations of a 5-membered ring according to the Cremer-Pople angle ϕ. B) Conformational FEL of isolated α-*L*-arabinofuranose. Conformations observed in Michaelis complexes of α-L–arabinofuranosidases are represented with a red star (PDB 2VRQ and 1QW9 for GH51 and PDB 6SXR, this work, for GH54). The conformational region having an equatorial O2 is shaded. C) Conformational FEL of α-L-arabinofuranose-configured cyclophellitol (**1**), aziridine (**2**) and cyclic sulfate (**6**).

RESULTS AND DISCUSSION

The free energy landscape of α-L-arabinofuranose, and the conformational itinerary of family GH51 and GH54 retaining α-L-arabinofuranosidases

To gain insight into the ability of our potential inhibitors to mimic the natural conformational preferences of α-L-arabinofuranosides, we computed the relative energy of all ring conformations of compounds **1**, **2**, and **6**. α-L-arabinofuranose was also analyzed for comparison. The conformational free energy landscape (FEL) of each molecule was calculated using *ab initio* metadynamics and the Cremer-Pople puckering coordinates. This approach has recently been successful in predicting the performance of pyranose-like inhibitors.[14,18]

In contrast to GHs which act on pyranosides (e.g. α/β-glucosidases[53] and α/β-mannosidases[54]), little is known about the catalytic conformational itineraries of α-L-arabinofuranosidases. The computed FEL of α-L-arabinofuranose (Figure 1B) shows that all conformations lie in an energy window of ≈ 5 kcal/mol. This window is significantly narrower than what is typical for pyranose compounds (≈ 15 kcal/mol)[41,55] and shows that most α-L-arabinofuranose conformations are thermally accessible. The most stable conformation is $^{1}T_{2}$. However, this conformation is not catalytically competent since the axial 2-OH group creates steric hindrance with the nucleophile residue located on the "beta" face of the sugar. Conformations between ^{2}E and ^{4}E, being only ≈ 2 kcal/mol higher in energy, feature an equatorial 2-OH, eliminating this steric hindrance. Thus, the ideal Michaelis complex conformation for an α-L-arabinofuranosidase should be between ^{2}E and ^{4}E (shaded region in Figure 1B).

To determine where on this landscape the observed conformations of enzyme-bound species lie, we surveyed all of the conformations of L-arabinofuranose observed within the active sites of crystallized GH51 and GH54 enzymes. Specific α-L-arabinofuranosidases have been identified within GH families 43, 51, 54, and 62, of which only families 51 and 54 follow the anomeric stereochemistry-retaining Koshland double-displacement mechanism.

The most detailed studies of α-L-arabinofuranosidase mechanisms have been performed using bacterial GH51 enzymes. Paes *et al.* obtained the structure of an intact branched pentasaccharide substrate bound to the active site of TxAbf, a thermostable GH51 from *Thermobacillus xylanilyticus* (PDB ID 2VRQ).[56] Hövel *et al.* reported the crystal structure of *Geobacillus stearothermophilus* AbfA (hereafter referred to as GsGH51) bound to 4-nitrophenyl α-L-arabinofuranoside (PNP-Araf) (PDB ID 1QW9).[57] In both of these Michaelis complexes, the α-L-arabinofuranose rings were found in the ^{4}E conformation (Figure 2A). Therefore, similar to observations with GHs acting on pyranose sugars[53], furanosidases distort the -1 sugar to a conformation that is pre-activated for catalysis. Thus, the conformational catalytic itinerary for the rate limiting step of the reaction for GH51 family is expected to go through an oxocarbenium ion-like E_3 conformer to fulfill the requirement of having C4-O5-C1-C2 planarity.[58]

Beyond the bacterial GH51 enzymes, there is only one retaining α-L-arabinofuranosidases which has been crystallized. The structure of *Aspergillus kawachii* AbfB (a member of GH54 hereafter referred to as AkAbfB) with arabinose in the active site (PDB ID 1WD4), displays a product complex ring conformation of ^{4}E.[59] Unfortunately, no Michaelis complex of this enzyme had been reported to date.

Determination of the Michaelis complex of AkAbfB

To complete, and thus compare the conformational itineraries of the GH51 and GH54 families, we studied AkAbfB as a model GH54 active site. To observe the Michaelis complex, we soaked

crystals of deglycosylated AkAbfB E221Q in a saturated solution of PNP-Araf in mother liquor. The resulting 1.64 Å crystal structure contained 3 PNP-Araf molecules: two full occupancy molecules bound to the carbohydrate binding module and a partial occupancy molecule bound in the active site (Supplemental Figure 6A).

Overall, the Michaelis complex displayed similarity to the product complex published by Miyanaga *et al.* in 2004[59] (Supplemental Figure 6B). O2 formed hydrogen bonds with the carbonyl oxygen of Q221 and the backbone amide of D297. O3 formed hydrogen bonds with the backbone amide of G296 and the carboxylate of D219. The ring oxygen formed a hydrogen bond with the backbone amide of N222 and O5 formed hydrogen bonds with the carboxylate of D219 and the backbone amide of N223. The furanose ring was found in a ^{4}E conformation, stacked against a hydrophobic surface formed by W206 and the C176-C177 disulfide linkage. The axial nitrophenyl leaving group pointed out of the active site into a solvent channel. The electrophilic carbon (C1) was positioned 3 Å away from the amide nitrogen, primed for migration away from the nitrophenyl leaving group with support from *anti* protonation of the glycosidic oxygen by D297, the general acid/base.

Based on this result, and the general observation of one itinerary per family (at least for members active on similar substrates),[54] we infer that enzymes within GH54 and GH51 share a common catalytic conformational itinerary (Figure 2A). Following binding in a reactive ^{4}E conformation, the glycone is predicted to pass through an E_3 transition state conformation to give a ^{2}E glycosyl-enzyme intermediate. Following exchange of the leaving group with water, the glycone then passes through a second E_3 transition state to form a lower energy product-bound complex observed in the low energy $E_3 - {}^4T_3$ region. Therefore, the predicted conformational itinerary for the two half-reactions is $^4E \rightarrow [E_3]^{\ddagger} \rightarrow {}^2E$ (glycosylaton) and $^2E \rightarrow [E_3]^{\ddagger} \rightarrow E^3/{}^4T_3$ (deglycosylation), as shown in Figure 2.

Conformational analysis of potential α-L-arabinofuranosidase inhibitors

Having ascertained the FEL for α-L-arabinofuranose and the conformational itinerary of retaining α-L-arabinofuranosidases, we next considered the design and synthesis of covalent inhibitors. As discussed above, both GH51 and GH54 enzymes form Michaelis complexes in the ^{4}E conformation (red stars in Figure 1B). Therefore, a suitable covalent α-L-arabinofuranosidase inhibitor should readily adopt a ^{4}E conformation in which the atom that mimics the anomeric carbon is similarly accessible for nucleophilic attack from the beta face of the sugar ring. Computed FELs for compounds **1**, **2**, and **6** (Figure 1C) show that these conformations are energetically favored for **6**, whereas **1** and **2** instead prefer conformations in which the 2-OH is axial (in the $^1T_2 - E_2 - {}^3T_2$ region). Thus, cyclic sulfate **6** was anticipated to be a potentially more potent inhibitor than the epoxide (**1**) or aziridine (**2**) for both GH51 and GH54 α-L-arabinofuranosidases.

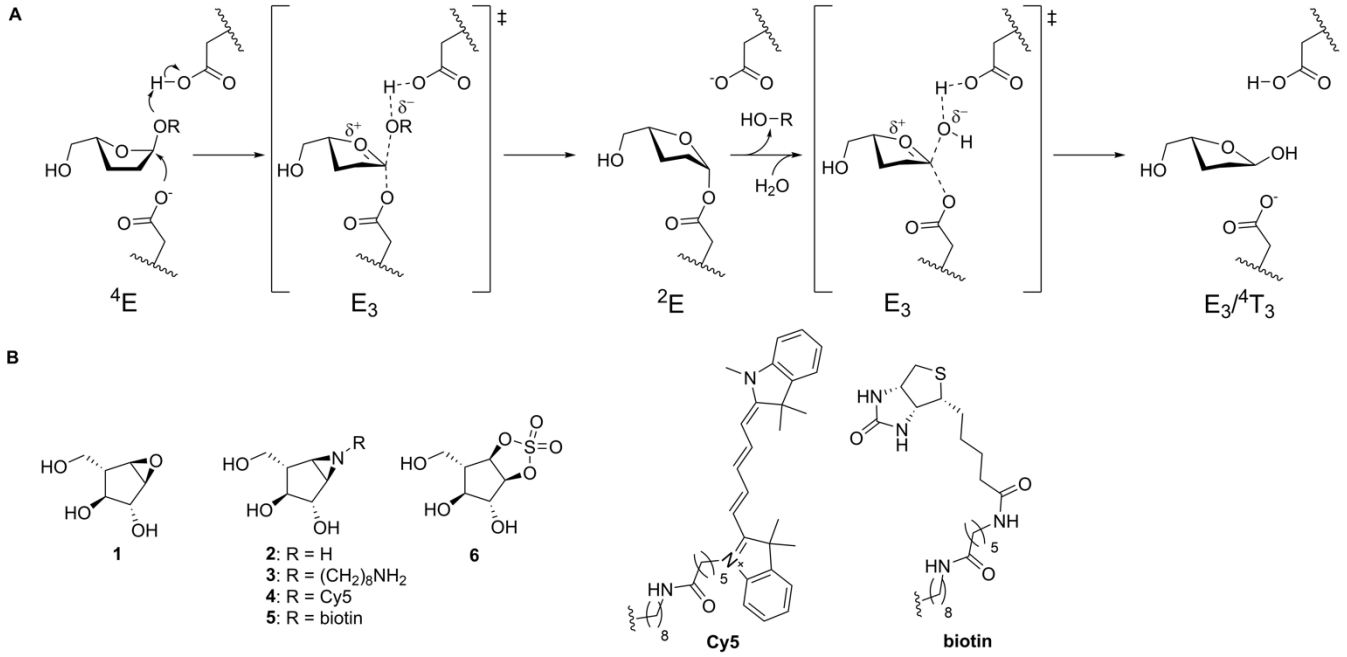

Figure 2. A) Koshland double-displacement mechanism employed by retaining α-L-arabinofuranosidases, as proposed for GH51 and GH54, showing the conformational reaction itinerary including the (left-to-right) Michaelis complex, transition state 1, covalent substrate-enzyme intermediate, transition state 2, and the hydrolyzed product. B) Chemical structures of putative α-L-arabinofuranosidase inhibitors **1**, **2**, **3**, and **6**, and ABPs **4** and **5**.

Synthesis of α-L-arabinofuranose-configured inhibitors and ABPs

To synthesize α-L-arabinofuranosidase inhibitors, we took inspiration from the synthesis of six-membered cyclophellitol derivatives beginning from appropriately functionalized cyclohexene starting materials. α-L-arabinofuranose-configured cyclopentene was prepared in nine steps from commercial methyl α-D-galactopyranoside in 15% yield. The initial installation of a *p*-methoxybenzylidene acetal (PMP) at C4 and C6 of methyl α-D-galactopyranoside (carbohydrate numbering) by treatment with anisaldehyde dimethylacetal followed by benzylation at C2 and C3 to afford intermediate **7** gave 74% yield over 2 steps

(Scheme 1). Selective opening of the PMP-group in compound **7** with Bu_2BOTf and BH_3·THF, followed by nucleophilic substitution of the primary alcohol with iodine and Vasella fragmentation with activated zinc powder afforded intermediate **10** in 60% yield over three steps. We were able to scale this process up to 56 mmol with moderate yields. Wittig olefination of aldehyde **10** and subsequent ring-closing metathesis (RCM) with second generation Grubb's catalyst afforded **11**. The PMB group was then selectively removed with DDQ and intermediate **14** was obtained in 66% yield over 4 steps by subsequent alkylation with freshly synthesized Bu_3SnMeI. The key step, a Wittig-Still rearrangement of intermediate **14** with *n*-BuLi at -78°C, afforded the desired cyclopentene **15** in 68% yield.

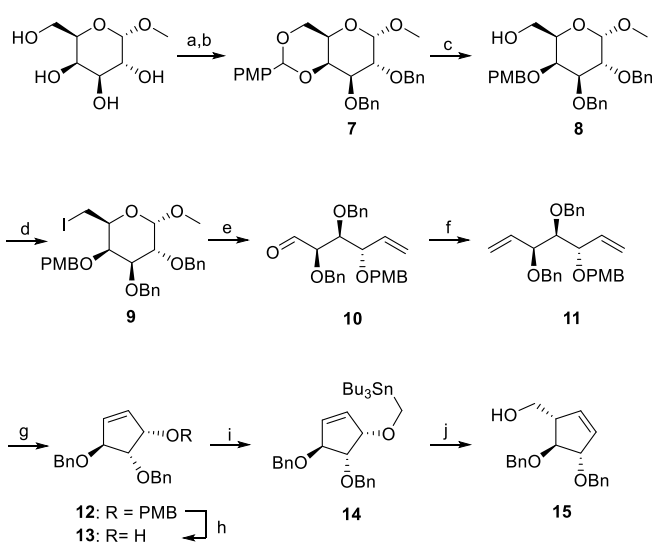

Scheme 1: Synthesis of L-arabinofuranose-configured cyclopentene **15**. Reagents and conditions: a) (1*S*)-(+)-10-Camphorsulfonic acid, CH_3CN, 50°C, 300 mbar, 2.5 h; b) BnBr, NaH, TBAI, DMF, 0°C, rt, 18 h, 74% over two steps; c) BH_3·THF, Bu_2BOTf, DMF, 0°C, 15 min, 90%; d) I_2, TPP, THF, reflux, 3 h, 79%; e) Activated Zn powder, THF, 35°C, 2 h, 84%; f) Ph_3PCH_3Br, *n*-BuLi, THF, -78°C to -20°C for 1 h, then rt, 18 h, 73%; g) Grubb's II cat., DCM, reflux, 18 h, 90%; h) DDQ, DCM, 0°C, rt, 2 h, 86%; i) Bu_3SnMeI, KH, dibenzo-18-crown-6, THF, 0°C, rt, 18 h, 91%; j) *n*-BuLi, THF, -78°C to rt, 18 h, 68%.

The first step towards the designed α-L-epoxide and α-L-aziridine compounds was stereoselective epoxidation of cyclopentene **15** (Scheme 2). We rationalized that treatment of cyclopentene **15** with *m*-CPBA would lead to predominant β-L-epoxidation where the neighboring primary alcohol would play a directing role by hydrogen bonding with *m*-CPBA. Indeed, *m*-CPBA epoxidation at 50°C overnight resulted in a separable 3.4:1 mixture of β-L- and α-L-epoxides in 62% yield. Cooling the mixture to 4°C slowed the reaction, and after 4 days, we observed a β-L to α-L ratio of 4.3:1, with a higher reaction yield (91%). To synthesize the α-L-epoxide selectively, cyclopentene **15** was benzylated and subjected to epoxidation with *m*-CPBA. Although the β-L to α-L ratio was improved to 1:2, it resulted in a chromatographically inseparable mixture. Thus, α-L-arabinofuranose-configured epoxide **1** was obtained by hydrogenation of partially benzylated **17** with Pearson's catalyst.

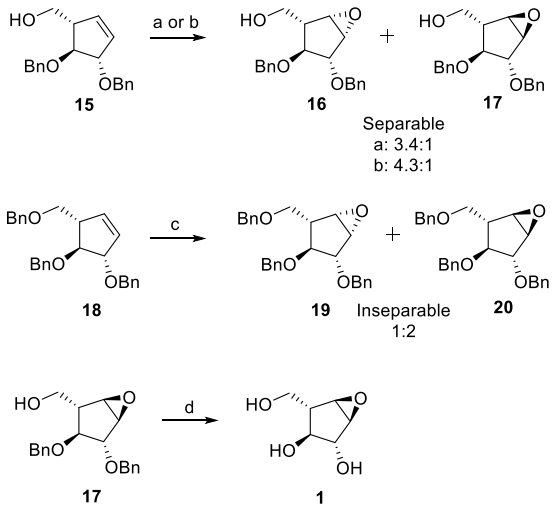

Scheme 2: Synthesis of epoxides. Reagents and conditions: a) *m*-CPBA, DCM, 50°C, 18 h, 62%, 3.4:1 of **16**:**17**. b) *m*-CPBA, DCM, 0°C, 4 days, 91%, 4.3:1 of **16**:**17**. c) *m*-CPBA, DCM, 50°C, 18 h, 62%, 1:2 of **19**:**20** d) H_2, $Pd(OH)_2$, MeOH, 18 h, 50%.

Taking advantage of the C2 and C4 stereochemistry of **18**, direct aziridination aided by steric hindrance of the vicinal protecting groups was attempted first. No aziridination was observed with 3-amino-2-(trifluoromethyl)quinazolin-4(3*H*)-one (Q-CF_3) as nitrogen donor and phenyliodine(III) diacetate (PIDA) to form the reactive acetylated quinazolinone.[60] *O*-(2,4-dinitrophenyl)hydroxylamine (DPH) and a ruthenium catalyst also gave no aziridination.[61] Hypothesizing that the alkene is not accessible enough due to the conformation of cyclopentene and/or steric hindrance of the benzyl groups, we pursued aziridine **2** by benzylation of the primary hydroxyl of epoxide **16** and subsequent S_N1 ring opening with sodium azide. This afforded two separable regio-isomers in 1:2 (**21**:**22**) ratio with 77% yield (Scheme 3). Hydroxyls of **21** and **22** were first tosylated and subsequently treated with triphenylphosphine (TPP) and diisopropylethylamine (DIPEA) at 60°C to obtain benzylated aziridine **23** in 28% yield over two steps. Aziridine **2** was obtained after deprotection under Birch conditions (sodium and *t*-butanol) with an overall yield of 11% from epoxide **16**. To synthesize ABPs, aziridine **23** was alkylated with 8-azidooctyl triflate. Following Birch deprotection, amino-octylaziridine **3** was obtained in 54% yield over two steps. Aziridine **3** was then coupled with either Cy5-OSu or biotin-OSu esters in the presence of DIPEA to afford ABPs **4** and **5** following HPLC purification.

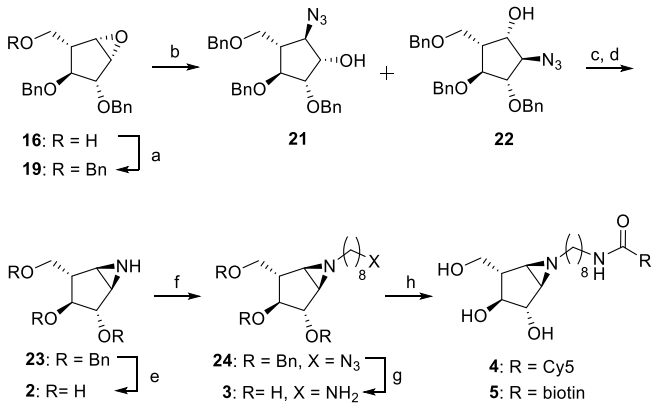

Scheme 3: Synthesis of α-L-aziridines **2-5**. Reagents and conditions: a) BnBr, NaH, TBAI, DMF, rt, 18 h, 78%. b) NaN_3, $LiClO_4$, DMF, 100°C, 18 h 77%. c) TsCl, DMAP, TEA, DCM, 0°C, 18 h, 50%. d) TPP, DIPEA, THF:H_2O, reflux, 1.5 h, 56%. e) Li, NH_3, -60°C, 1 h, 66%. f) 8-azidooctyl triflate, DIPEA, DCM, 0°C to rt, 18 h, 57%. g) Na, NH_3, t-BuOH, -60°C, 1 h, 95%. h) Cy5-Osu or biotin-OSu, DIPEA, DMF, 18 h, **4**: 56% and **5**: 19%.

The synthesis of irreversible α-L-arabinofuranose configured cyclic sulfate **6** (Scheme 4) started with the oxidation of **18** with a mixture of $NaIO_4$ and $RuCl_3{\cdot}3H_2O$ affording exclusively cis-α-L-diol **25** in 48% yield. Diol **25** was then treated with thionyl chloride and trimethylamine, and the sulfite mixture was then further oxidized with $NaIO_4$ and $RuCl_3{\cdot}3H_2O$ to give cyclic sulfate **26**. This was deprotected using Pearson's catalyst to afford final cyclic sulfate **6** in 24% yield from **18**.

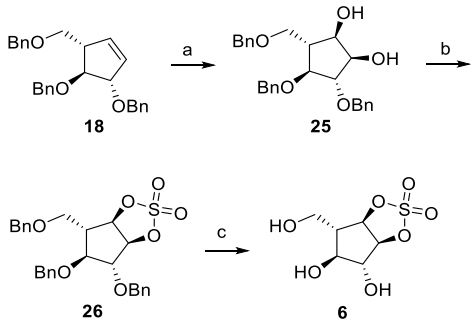

Scheme 4: Reagents and conditions towards cyclic sulfate **3**. a) $NaIO_4$, $RuCl_3{\cdot}3H_2O$, EtOAc/CH_3CN/H_2O, 0°C, 3 h, 48%. b) i) $SOCl_2$, Et_3N, DCM, 0°C, 30 min. ii) $NaIO_4$, $RuCl_3{\cdot}3H_2O$, EtOAc/CH_3CN/H_2O, 0°C, 3 h, 51% c) H_2, $Pd(OH)_2$, MeOH, 18 h, 24%.

Inhibition of recombinant α-L-arabinofuranosidases

With **1**, **2**, and **6** in hand, we first assessed the potency of these putative inhibitors against their intended targets. To test the effectiveness of each inhibitor, inhibition kinetics were measured with a collection of recombinantly produced retaining α-L-arabinofuranosidases including *Geobacillus stearothermophilus* GH51 (GsGH51, a bacterial enzyme from GH51), *Aspergillus niger* AbfA (AnAbfA, a fungal enzyme from GH51), and *Aspergillus kawachii* AbfB (AkAbfB, a fungal enzyme from GH54). Initial overnight incubations of each enzyme with compounds **2** and **6** resulted in the complete loss of activity, while no loss of activity was observed with compound **1**. Intact MS of GsGH51 and AkAbfB treated with each compound confirmed complete 1:1 labelling with compounds **2** and **6**, and no labelling with compound **1** (Supplemental Figure 7, Supplemental Figure 8).

AnAbfA (GH51)			
Compound	K_I (μM)	k_{inact} (min^{-1})	k_{inact}/K_I ($s^{-1}M^{-1}$)
1	n.d.	n.d.	<0.1
2	140±20	0.33±0.02	39
3	210±30	0.09±0.01	7.1
6	n.d.	n.d.	160±20
AkAbfB (GH54)			
1	n.d.	n.d.	<0.1
2	320±50	0.54±0.07	28
3	320±40	0.12±0.01	6.2
6	n.d.	n.d.	240±30

Table 1: Kinetic parameters for covalent inhibition of AnAbfA and AkAbfB by α-L-arabinofuranosidase compounds **1**, **2**, **3**, and **6**. For reactions with compound **6**, it was not possible to obtain distinct k_{inact} and K_I parameters; only the combined k_{inact}/K_I parameter determined from the slope of the k_{app} vs [I] curve is shown for these cases. n.d.: not determined.

As predicted by our conformational analysis, compound **6** is a potent inhibitor of retaining α-L-arabinofuranosidases. Inhibitor **6** reacted rapidly with the catalytic nucleophile of both AkAbfB and AnAbfA with a k_{inact} well above 1 min^{-1} (estimated from the limited speed of our assay). However, the lack of any apparent non-linearity in the k_{app} vs. [I] curve for either AkAbfB or AnAbfA suggested poor initial binding (Supplemental Figure 1**Error! Reference source not found.**, Supplemental Figure 2**Error! Reference source not found.**). In spite of this, inhibitor **6** has a performance constant of 170 $M^{-1}s^{-1}$ with AnAbfA and 250 $M^{-1}s^{-1}$ with AkAbfB (Table 1), comparable to the inhibition of TmGH1 with cyclophellitol reported by Gloster *et al.*[11] (290 $M^{-1}s^{-1}$).

Contrary to our prediction, compound **2** also proved to be a potent inhibitor of both AkAbfB and AnAbfA, having performance constants only 8-fold and 4-fold lower than inhibitor **6** with AkAbfB and AnAbfA, respectively (Table 1). In contrast to inhibitor **6**, inhibition kinetics with inhibitor **2** provided evidence of stronger initial binding in both enzyme active sites, having K_I values of 0.1-0.3 mM. The addition of an alkyl chain to generate inhibitor **3** did not hinder initial binding with either AnAbfA or AkAbfB and caused only a 4-fold reduction in k_{inact}, demonstrating that alkylation of the aziridine is a well-tolerated method for generating α-L-arabinofuranosidase ABPs.

The lack of measurable inhibition kinetics for compound **1** allowed us to establish a maximum value for the putative inhibitor's performance constant (k_{inact}/K_I) of approximately 0.1 $M^{-1}s^{-1}$ based on the length and sensitivity of the assay and the maximum inhibitor concentration tested (Supplemental Figure 1**Error! Reference source not found.**, Supplemental Figure 2**Error! Reference source not found.**). Similarly, no reversible inhibition was observed at concentrations as high as 0.25 mM. Together, these results confirmed that, as predicted from our conformational analysis, compound **1** was not an inhibitor of retaining α-L-arabinofuranosidases at concentrations up to 0.25 mM.

Structural analysis of inhibitors 2 and 6 bound to α-L-arabinofuranosidases

To determine whether inhibitors **2** and **6** both interact with α-L-arabinofuranosidases as effective α-L-arabinofuranose mimics, we sought to understand how the inhibitors bind to the enzyme

active site. Soaking GsGH51 with inhibitors **2** and **6** overnight at room temperature resulted in the formation of full occupancy covalent complex between E294, the known catalytic nucleophile, and each inhibitor (Figure 3A,B). These structures are similar to the complexes reported by Hövel *et al.*[57] They reported a covalent substrate-enzyme intermediate trapped in a ^{2}E conformation (PDB ID 1PZ2); however, poor electron density at the anomeric center of the Hövel structure limits the confidence with which this ligand conformation can be interpreted. Nevertheless, it is clear that the structure of the active site varies between the Hövel complexes and the complexes with inhibitors **2** and **6** that we obtained (Supplemental Figure 9).

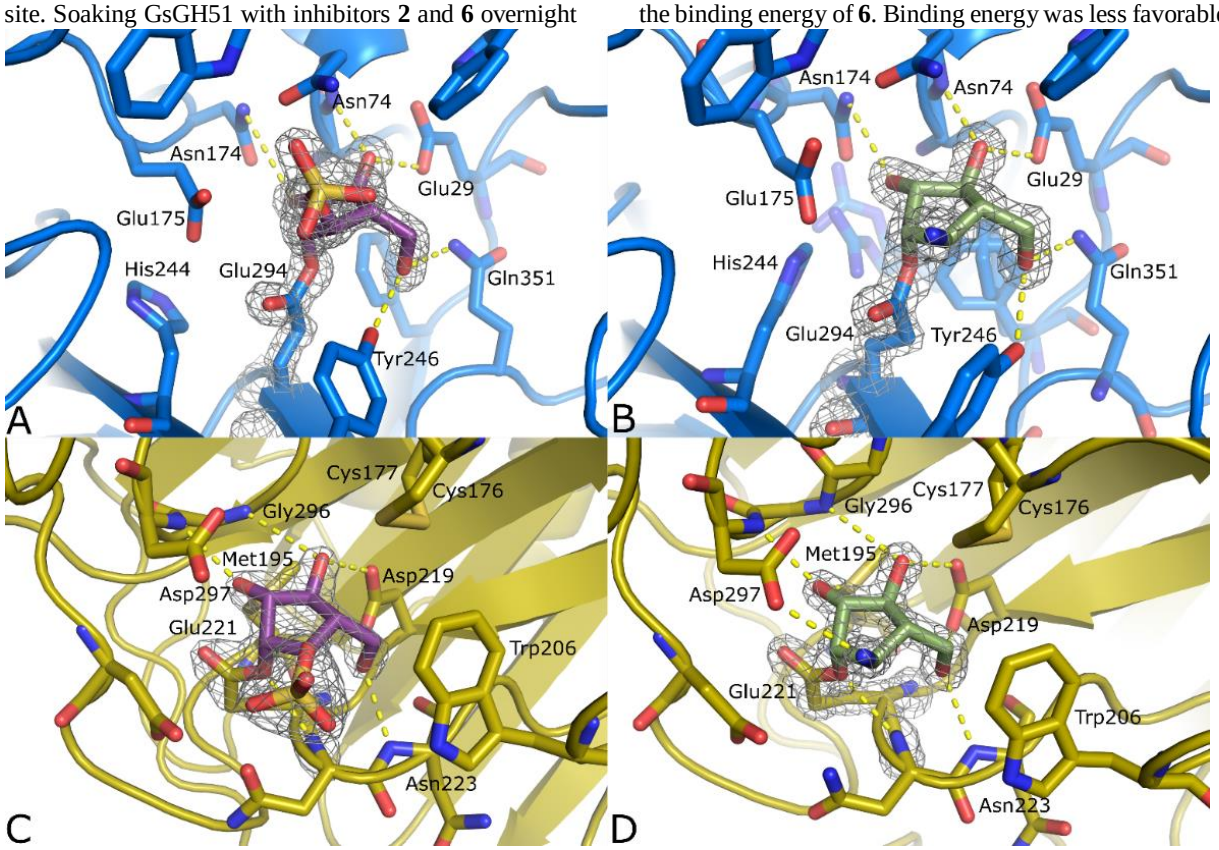

Figure 3. Crystal structures of complexes between inhibitors **2** (B, D, green) and **6** (A, C, purple), and GsGH51 (A, B, blue) and AkAbfB (C, D, yellow). $2F_o$-F_c electron density is shown for both the ligand and the catalytic nucleophile as a grey mesh contoured at 2σ. The polypeptide is shown in cartoon form with active site residues shown as sticks. Apparent hydrogen bonding interactions are shown as dotted yellow lines.

Complexes with both inhibitors **2** and **6** are characterized by the positioning of the E294 side chain away from R69, towards the unliganded (PDBID: 1PZ3) position of Y246, which, in place of a hydrogen bond to the ring oxygen of α-L-arabinofuranose, forms a hydrogen bond with O5 of the inhibitor (carbohydrate numbering). While the resulting displacement of Y246 has only a minimal impact on the protein structure when bound to inhibitor **6,** binding to inhibitor **2** results in the dramatic displacement of Y246, and consequently W298 and N302, creating sufficient space for the sidechains of I356 and L318 to pack into a different position and for a glycerol molecule to bind. The presence of the bulky charged sulfate group following reaction with inhibitor **6** appears to repel E175, the general acid/base residue, displacing H244 and, through steric interactions, the S215-R218 loop. To investigate whether E175 is interfering with the binding of inhibitor **6**, we simulated the Michaelis complex of inhibitor **6** with the E175A and E175G mutants, and calculated the binding energy of **6**. Binding energy was less favorable with either mutant (+4 kcal/mol for E175A and +8 kcal/mol for E175G). We interpret this as indicating that the displacement of E175 likely occurs following the reaction of the cyclic sulfate with the covalent nucleophile. We speculate that the observed active site rearrangement occurs following the addition reaction and is not relevant to initial inhibitor binding. Overall, while inhibitors **2** and **6** both bind in a manner mimicking the cognate substrate of GsGH51, their labelling of the catalytic nucleophile appears to induce significant rearrangement of the active site structure.

Interestingly, following reaction with the catalytic nucleophile, the conformation of inhibitor **2**, but not inhibitor **6**, appears to represent the glycone conformation expected of the glycosyl enzyme intermediate. Reacted inhibitor **2** was found in the ^{2}E conformation, forming hydrogen bonds from O2 to N174, from O3 to N74 and E29, and from O5 to Q351 and Y246. Inhibitor **6** formed the same complement of ligand-protein interactions but sat in the active site in an unusual E_1 conformation. We attribute this to a combination of electrostatic repulsion and steric bulk pushing the sulfate group out of the active site, promoting an extended conformation for the bonds connecting Oε1 of E294 to the sulfate group.

To generate covalent GH54 complexes, we soaked crystals of AkAbfB with 0.2 mM of inhibitor **2** or **6** for 1 hour. Both inhibitors bound to E221 in almost identical positions and conformations (Figure 3C,D), forming hydrogen bonds from O2 to G296 and the sulfur of M195, from O3 to N297 and D219, and

from O5 to D219 and N223. The interaction between the ring oxygen and N222 found in the product complex (PDBID: 1WD4) cannot be formed, but the axial amine presents an additional hydrogen bond with D297, the general acid/base. In contrast to the complex with GsGH51, the interactions between both inhibitors **2** and **6** and the active site of AkAbfB cause no significant change in the protein structure. The active site appears to be sufficiently open to accommodate the sulfate of inhibitor **6** without any steric clashes. Thus, we believe that these complexes are good representations of the glycosyl-enzyme intermediate structure. The ring in each covalent complex is found in the ^{2}E conformation. This consensus conformation represents a 1.2 Å migration of C1 from its position in the AkAbfB Michaelis complex toward E221 coupled with a ~15° axial rotation of the ring around C3 (Supplemental Figure 10).

Probing the *Aspergillus niger* arabinan secretomes with ABP 4

Building on the success of inhibitors **2** and **3** as covalent inhibitors of both GH51 and GH54 α-L-arabinofuranosidases, we set out to detect and identify α-L-arabinofuranosidases within complex fungal secretomes. As a validation of this approach, we chose to work with the well-studied secretome of *A. niger* grown on arabinan.

Multiple α-L-arabinofuranosidases have been purified from the *A. niger* secretome and characterized.[62–64] These include AnAbfA, the fungal GH51 that we produced recombinantly, and AnAbfB, a GH54 enzyme 98% identical to AkAbfB. Thus, we hypothesized that our ABPs could be used to identify the α-L-arabinofuranosidases that are produced by *A. niger* in response to a specific carbon source.

The treatment of the *A. niger* arabinan secretome with inhibitor **2** resulted in the complete loss of activity against 4MU-Araf, suggesting that all of the α-L-arabinofuranosidase activity in our secretome sample could be attributed to retaining glycosidases.

Visualization of α-L-arabinofuranosidases using ABP **4** revealed two distinct bands, one running at ~105 kDa and the other running at ~65 kDa (Figure 4A). Deglycosylation with PNGaseF under denaturing conditions resulted in a shift of the 105 kDa band down to ~70 kDa and a shift of the ~65 kDa band down to ~60 kDa. Based on similar results obtained with recombinant AnAbfA and AkAbfB, we hypothesized that the top band was one of the *A. niger* GH51 enzymes and the bottom band was AnAbfB, the only *A. niger* GH54 enzyme.

Investigations of the effects of pH on labelling efficiency revealed that AnAbfB reacted with our probe efficiently over a pH range (2-9), which extended further into the acidic range than the GH51 enzyme (5-8) (Supplemental Figure 11). Notably, both enzymes were labelled optimally at pH 6.5-7, which is significantly above pH 4, at which the enzymes are optimally active. While similar discrepancies between optimal hydrolytic and inhibition pH have been reported previously[15,18], the difference of 2.5-3 pH units that we observed is unusually large, suggesting that the optimal protonation states of active site residues for inhibition by compound **2** and glycoside hydrolysis are different.

This is supported by the trends observed in the binding energies calculated for the modelled Michaelis complexes of inhibitor **1**, **2,** and **6** in the GH51 and GH54 active sites (Supplemental Figure 12, Supplemental Figure 13). The binding energy of inhibitor **2** was calculated in 3 different situations in each active site: deprotonated inhibitor **2** with protonated acid/base residue, protonated inhibitor **2** with protonated acid/base residue, and protonated inhibitor **2** with deprotonated acid/base residue. Protonated compound **2** (with the optimal acid/base residue protonation) binds better than all the other compounds in both enzymes (Supplemental Figure 14**Error! Reference source not found.**); thus, not requiring the donation of a proton from the general acid/base residue for the reaction to take place. Also, the importance of the protonation state of the acid/base residue seems to be different in both enzymes. GH54 with an extended acidic range of labelling efficiency seems to have similar binding energies with either the protonated or deprotonated general acid/base; whereas in GH51, **2** binds much better when it is deprotonated, explaining the more restricted pH range of labelling efficiency.

To investigate the thermal stability of arabinofuranosidases within the *A. niger* arabinan secretome, we pre-incubated the secretome at various temperatures for one hour prior to visualization with ABP **4**. This revealed enzyme recovery from surprisingly high temperature treatments (Supplemental Figure 15A,C). Both enzymes were stable up to 60°C. Increasing the temperature to 65°C resulting in a complete loss of GH54 staining and raising it to 67°C resulted in a complete loss of both GH51 and GH54 labeling, suggesting complete denaturation. However, increasing the pre-incubation temperature beyond 67°C resulted in a partial recovery of GH54 staining. Pre-incubation at 86.5°C resulted in a ~50% recovery of fluorescence intensity relative to the RT control (estimated by band integration using ImageQuant software (GE)). To determine the role of disulfide bonding in the stability AbfA and AbfB and the apparent refolding of AbfB, we repeated the experiment with 5 mM DTT (Supplemental Figure 15B,C). The addition of DTT had minimal impact on the apparent stability of AbfA, yet significantly reduced the apparent stability of AbfB, causing a near complete loss of staining at 56°C. This suggests that the four disulfide bonds found in the structure of AkAbfB (conserved in AnAbfB) are critical for enzyme stability, but that disulfide bonds are not important for AbfA stability. Enzyme recovery from elevated temperatures was reduced, but still occurred in spite of the reduction of disulfide bonds.

To determine whether the recovery of AbfB staining was genuinely related to the recovery of active enzyme, we measured hydrolytic activity of the DTT treated secretome samples towards 4MU-Araf (Supplemental Figure 15D). This confirmed that the loss of AbfB staining at 56°C correlated with an ~80% reduction in activity and that the subsequent loss of AbfA staining at 67°C corresponded with a complete loss of activity. At higher temperatures we observed a small recovery of activity which correlated with the recovery of AbfB staining. Thus, visualization with ABP **4** facilitates the identification of thermally resilient enzymes within the context of their native fungal secretome.

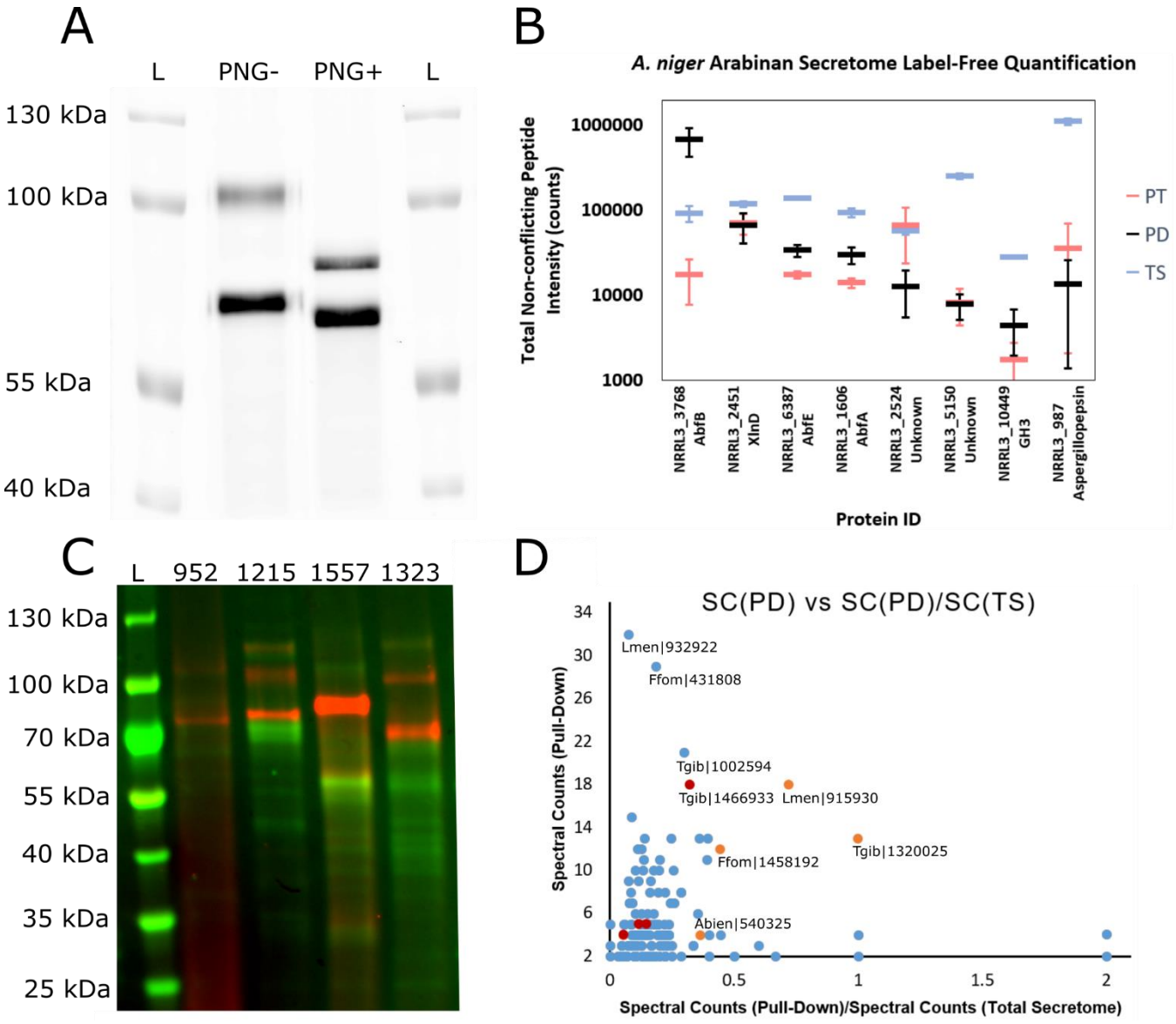

Figure 4. Activity-based protein profiling of fungal secretomes with ABPs **4** and **5**. A) Fluorescence imaging of the secretome isolated from *A. niger* grown on arabinan, stained with ABP **4**, and treated with (PNG+) or without (PNG-) PNGaseF under denaturing conditions prior to separation on an 8.75% SDS-PAGE gel. L indicates the ladder lanes. B) Label-free quantification of the top eight proteins pulled down from the *A. niger* arabinan secretome. For each protein (identified by NRRL3 number and common name), integrated peptide intensity is plotted for non-conflicting peptides from the pull-down with ABP **5** (PD, black), from the total secretome (TS, blue), and from the pull-down with ABP **5** following pre-treatment with inhibitor **2** (PT, red). Error bars represent the standard deviations of three measurements. C) Cy5 fluorescence (red) and Coomassie staining (green) of basidiomycete secretomes following staining with ABP **4** and acetone precipitation. L indicates the ladder lane. The BRFM number for the strain from which the secretome was isolated is given above each lane. D) Plot of total spectral counts in the pull-down sample vs. the ratio of spectral counts in the pull-down sample to spectral counts in the total secretome for all of the proteins for which at least 2 peptides were observed with an FDR of 1% in the pull-downs from *L. menziesii* (BRFM 1557), *F. fomentarius* (BRFM 1323), *T. gibbosa* (BRFM 952), and *A. biennis* (BRFM 1215). Points corresponding to GH51 enzymes are shown in orange, points corresponding to other putative retaining GH enzyme with peptide molecular weights >90 kDa are shown in red. The labels shown include the species abbreviation and the Mycocosm amino acid sequence number.

Identification of *A. niger* α-L-arabinofuranosidases by pull-down with ABP 5

Based on molecular weight and glycosylation state, we hypothesized that the enzymes stained by ABP **4** were a GH51 and a GH54. However, it was not clear which of the GH51 enzymes produced by *A. niger* was expressed. A previous report has identified AbfA, AbfB, and AbfC as the major α-L-arabinofuranosidases produced by *A. niger* in response to growth on arabinan-rich sugar beet pectin[62]. The genome of *A. niger* encodes two other GH51 genes: abfD, which is not expressed during growth on arabinan, and the more recently identified abfE, for which expression has not been investigated in response to arabinan.

On-bead digestion of proteins pulled down following treatment of the secretome with ABP **5** yielded peptides from AbfB (GH54, GenBank: CAK42333), AbfA (GH51, GenBank:

CAK43424), and AbfE (GH51, GenBank: ACE00420) as well as a small collection of other proteins not known to be α-L-arabinofuranosidases (Figure 4B). We did not observe AbfC or AbfD in our analysis of the pull-down total secretome, indicating that these were not produced in our culture. Pre-incubation of the secretome with inhibitor **2** followed by treatment with ABP **5** and pull-down significantly reduced signal for peptides from AbfA, AbfB, and AbfE without causing a significant reduction in signal for any other detected proteins. Although we cannot exclude that ABP **5** has specific targets beyond arabinofuranosidases that are incapacitated by inhibitor **2**, these results reveal the utility of ABP **5** in activity-based protein profiling to identify and annotate retaining arabinofuranosidases from secretomes derived from microorganisms grown on arabinofuranose-containing biopolymers.

Screening basidiomycetes for α-L-arabinofuranosidase production

Following the success of the detection and identification of *A. niger* α-L-arabinofuranosidases, we applied ABPs **4** and **5** to the detection and identification of α-L-arabinofuranosidases secreted by basidiomycetes grown on complex biomass. We selected a sampling of eight basidiomycetes, all known to be proficient biomass-degrading fungi (Supplemental Table 3). The genomes of these fungi encode no apparent GH54 enzymes and either one (*A. biennis* and *T. gibbosa*) or two apparent GH51 enzymes. To identify the GH51(s) produced during growth on complex biomass, these fungi were cultured on maltose, aspen pulp, or wheat straw for 10 days prior to secretome collection.

α-L-Arabinofuranosidases were visualized by treatment of secretome samples with ABP **4** at pH 5.5, 30°C for 1 hour followed by denaturation, deglycosylation, and separation on SDS-PAGE. Glycoproteins migrating at 70-80 kDa were observed in secretomes collected from *T. gibbosa* (the top biomass digestion-enhancing strain identified in a sampling of French biomass-degrading fungi[65]), *F. fomentarius* (a white-rot fungus which grows on hardwood trees[66]), and *L. menziesii* and *A. biennis* (both known to be effective in biomass pre-treatment[67,68]) when grown on aspen pulp (Supplemental Figure 16A). *T. gibbosa* and *L. menziesii* secretomes gave the same band following growth on wheat straw while the secretomes of *A. biennis* and *F. fomentarius* did not (Supplemental Figure 16B). *T. gibbosa*, *F. fomentarius*, and *A. biennis* did not produce any apparent α-L-arabinofuranosidase when grown on maltose. However, surprisingly, *L. menziesii* did. Coomassie staining showed very little total protein present in any of the secretome samples (Supplemental Figure 16C, D), demonstrating the remarkable sensitivity of ABP **4**.

Based on these results, *T. gibbosa*, *L. menziesii*, *A. biennis*, and *F. fomentarius* were selected for follow-up studies. Staining 100 μL of secretome followed by acetone precipitation gave much higher band intensity compared to the effective loading of ~2.8 μL in the screening experiment. This revealed a collection of 1-3 bands running between 55 and 130 kDa (Figure 4C, and Supplemental Figure 17). Coomassie staining of the same gel revealed a broad range of bands, few of which appeared to co-migrate with the bands detected by visualization with ABP **4** (Figure 4C).

Bands stained with ABP **4** in these samples were identified by pull-down using the same protocol as for the *A. niger* secretome, but with an added 10-minute wash of the beads with 2% SDS at 65°C to more strictly eliminate any proteins non-specifically bound to the beads. Comparing proteomic analyses of the secretome and pull-down samples, the vast majority of proteins found within the secretome were rendered undetectable by our washing protocol. In spite of this, the proteins confidently observed (at least two unique peptides identified with an FDR of 1%) were still predominantly not enzymes phylogenetically related to known α-L-arabinofuranosidases. Considering the abundance of GH7 enzymes apparent in the total secretome and in the pull-down, and the apparent staining of the same enzymes by ABP **4** (~50-60 kDa bands in Figure 4C), we believe that many of these hits represent non-specific labelling of abundant species within the secretome (e.g. GH7 enzymes Lmen|932922, Ffom|431808, and Tgib|1002594).

Thus, we combined the metrics of total spectral counts from the pull-down (SC(PD), a rough measure of abundance) and the ratio of spectral counts from the pull-down to spectral counts from the digestions of the total secretome (SC(PD)/SC(TS), a rough measure of selectivity) to give the plot shown in Figure 4D. Three GH51 enzymes (JGI ProtIDs Lmen|915930, Tgib|1320025, and Ffom|1458192) appear as distinct targets of ABP **5** with elevated SC(PD) and SC(PD)/SC(TS). These GH51 enzymes had masses correlated with the masses of the most intense bands observed by visualization with ABP **4** (those between 70 and 100 kDa). A single GH51 enzyme in the same mass range from *A. biennis* (Abien|540325) was detected in the pull-down sample. However, the signal was weak, with only 4 spectral counts detected.

Based on the limited number of hits in the pull-down samples with predicted molecular weights above 90 kDa, we believe that the higher molecular weight bands (100-120 kDa) observed in the SDS-PAGE of secretomes from *T. gibbosa*, *A. biennis*, and *F. fomentarius* are GH3, GH31, or GH35 enzymes. Most of these enzymes were observed with poor SC(PD) and SC(PD)/SC(TS) values (red dots in Figure 4D), however a single GH3 enzyme (Tgib|1466933) appeared to be a target of ABP **5**. While this may represent substrate flexibility within these GH families, it remains to be determined whether these enzymes display significant α-L-arabinofuranosidase activity.

CONCLUSIONS

The discovery of the mechanism-based covalent α-L-arabinofuranosidase inhibitors **2** and **6** expand the library of tools available for the characterization of enzymes expressed during plant biomass degradation. The unexpectedly high efficiency of inhibitors **2** and **3** provided a platform on which ABPs for α-L-arabinofuranosidases could be synthesized. The potential of ABPs **4** and **5** in the discovery, identification, and characterization of α-L-arabinofuranosidases from fungal secretomes grown on both arabinose-rich biomass and complex woody biomass has been demonstrated. We envision that the ability to efficiently screen samples of interest for levels of multiple active α-L-arabinofuranosidases will facilitate and accelerate a variety of applications including enzyme discovery, bioprocess monitoring, and the investigation of plant-pathogen interactions.

ASSOCIATED CONTENT

Supporting information for this article includes:
-Supplemental figures and table
-Supplemental synthetic methods and characterization for compounds **1-23**
This material is available free of charge via the Internet at http://pubs.acs.org

Crystallographic structural models and diffraction data can be accessed at www.rcsb.org under the PDB IDs 6SXV, 6SXU, 6SXT, 6SXS, and 6SXR.

Proteomic LC-MS/MS datasets have been deposited with the MassIVE database (massive.ucsd.edu, UCSD) with the identifiers MSV000084886 (*A. niger* arabinan secretome) and MSV000084877 (Basidiomycete secretomes) and can be accessed via FTP.

AUTHOR INFORMATION

Corresponding Author

*Correspondence should be addressed to HSO <h.s.overkleeft@lic.leidenuniv.nl>, CR <c.rovira@ub.edu> or GJD <gideon.davies@york.ac.uk>

Funding Sources

We thank the Natural Sciences and Engineering Research Council of Canada (Post-Doctoral Fellowship to NGSM), the Royal Society (Ken Murray Research Professorship to GJD), the Biotechnology and Biological Sciences Research Council (BBSRC) (grant BB/R001162/1 to GJD), the Netherlands Organization for Scientific Research (NWO TOP grant 2018-714.018.002 to HSO), the European Research Council (ERC-2011-AdG-290836 "Chembiosphing" to HSO), the Generalitat de Catalunya (FI-AGAUR PhD scholarship to AN-H), the computer resources at MareNostrum IV and MinoTauro and the technical support provided by the Barcelona Supercomputing Center (BCV-2016-2-0002 and BCV-2016-3-0005), and the computational support from the University of York High Performance Computing service, Viking and the Research Computing team (chem-menz-2019). Joint Genome Institute, a DOE Office of Science User Facility, is supported by the Office of Science of the U.S. Department of Energy under Contract No. DE-AC02-05CH11231. The authors declare no competing financial interest.

ACKNOWLEDGMENT

The authors would also like to thank professors Takuya Koseki and Shinya Fushinobu for providing the expression plasmid for AkAbfB. The authors would like to thank Diamond Light Source for beam time (proposal 18598), and the staff of beamline I04 for assistance with crystal testing and data collection. Proteomics data were collected at the York Centre of Excellence in Mass Spectrometry, which was created thanks to a major capital investment through Science City York, supported by Yorkshire Forward with funds from the Northern Way Initiative, and subsequent support from EPSRC (EP/K039660/1; EP/M028127/1). Wiley-milled aspen (*Populus grandidentata*) was kindly provided by Dan Cullen (Forest Product Laboratory, USDA, Madison, WI, USA). The authors are grateful to Igor V Grigoriev, Joint Genome Institute for providing access to genome sequence data for *Trametes gibbosa* BRFM 1770, *Abortiporus biennis* BRFM 1778, *Hexagonia nitida* BRFM 1802, *Trametes ljubarskyi* BRFM 1659, *Leiotrametes menziesii* BRFM 1781, *Fomes fomentarius* BRFM 1823 and *Trametes meyenii* BRFM 1810.

ABBREVIATIONS

4MU-Araf: 4-methylumbelliferyl α-L-arabinofuranoside
a.u.: Atomic units
ABP: Activity-based probe
CP: Car-Parrinello
DDQ: 2,3-Dichloro-5,6-dicyano-1,4-benzoquinone
DIPEA: Diisopropylethylamine
DPH: *O*-(2,4-dinitrophenyl)hydroxylamine
FEL: Free-energy landscape
GH51: Glycoside hydrolase family 51
GH54: Glycoside hydrolase family 54
MD: Molecular dynamics
PD: Pull-down
PIDA: Phenyliodine(III) diacetate
PNP-Araf: 4-nitrophenyl α-L-arabinofuranoside
PMB: Para-methoxybenzyl
PMP: Para-methoxybenzylidene
RCM: Ring-closing metathesis
SC: Spectral counts
SD: Standard deviation
SPG: Succinate-phosphate-glycine
TPP: Triphenylphosphine
TS: Total secretome
Q-CF_3: 3-amino-2-(trifluoromethyl)quinazolin-4(3*H*)-one

REFERENCES

(1) Lombard, V.; Golaconda Ramulu, H.; Drula, E.; Coutinho, P. M.; Henrissat, B. The Carbohydrate-Active Enzymes Database (CAZy) in 2013. *Nucleic Acids Res.* **2014**, *42* (D1), D490–D495.

(2) Miyauchi, S.; Navarro, D.; Grisel, S.; Chevret, D.; Berrin, J. G.; Rosso, M. N. The Integrative Omics of White-Rot Fungus Pycnoporus Coccineus Reveals Co-Regulated CAZymes for Orchestrated Lignocellulose Breakdown. *PLoS One* **2017**, *12* (4), e0175528.

(3) Williams, S. J.; Hekmat, O.; Withers, S. G. Synthesis and Testing of Mechanism-Based Protein-Profiling Probes for Retaining Endoglycosidases. *ChemBioChem* **2006**, *7* (1), 116–124.

(4) Hekmat, O.; Kim, Y. W.; Williams, S. J.; He, S.; Withers, S. G. Active-Site Peptide "Fingerprinting" of Glycosidases in Complex Mixtures by Mass Spectrometry: Discovery of a Novel Retaining β-1,4-Glycanase in Cellulomonas Fimi. *J. Biol. Chem.* **2005**, *280* (42), 35126–35135.

(5) Hekmat, O.; He, S.; Warren, R. A. J.; Withers, S. G. A Mechanism-Based ICAT Strategy for Comparing Relative Expression and Activity Levels of Glycosidases in Biological Systems. *J. Proteome Res.* **2008**, *7* (8), 3282–3292.

(6) Chauvigné-Hines, L. M.; Anderson, L. N.; Weaver, H. M.; Brown, J. N.; Koech, P. K.; Nicora, C. D.; Hofstad, B. A.; Smith, R. D.; Wilkins, M. J.; Callister, S. J.; Wright, A. T. Suite of Activity-Based Probes for Cellulose-Degrading Enzymes. *J. Am. Chem. Soc.* **2012**, *134* (50), 20521–20532.

(7) Liu, Y.; Fredrickson, J. K.; Sadler, N. C.; Nandhikonda, P.; Smith, R. D.; Wright, A. T. Advancing Understanding of Microbial Bioenergy Conversion Processes by Activity-Based Protein Profiling.

Biotechnol. Biofuels **2015**, *8* (1), 156.

(8) Wu, L.; Armstrong, Z.; Schröder, S. P.; de Boer, C.; Artola, M.; Aerts, J. M.; Overkleeft, H. S.; Davies, G. J. An Overview of Activity-Based Probes for Glycosidases. *Curr. Opin. Chem. Biol.* **2019**, *53*, 25–36.

(9) Rosnow, J. J.; Anderson, L. N.; Nair, R. N.; Baker, E. S.; Wright, A. T. Profiling Microbial Lignocellulose Degradation and Utilization by Emergent Omics Technologies. *Critical Reviews in Biotechnology*. July 4, 2017, pp 626–640.

(10) Kuo, C. L.; van Meel, E.; Kytidou, K.; Kallemeijn, W. W.; Witte, M.; Overkleeft, H. S.; Artola, M. E.; Aerts, J. M. *Activity-Based Probes for Glycosidases: Profiling and Other Applications*; Academic Press, 2018; Vol. 598, pp 217–235.

(11) Gloster, T. M.; Madsen, R.; Davies, G. J. Structural Basis for Cyclophellitol Inhibition of a β-Glucosidase. *Org. Biomol. Chem.* **2007**, *5* (3), 444–446.

(12) Jiang, J.; Kuo, C. L.; Wu, L.; Franke, C.; Kallemeijn, W. W.; Florea, B. I.; Van Meel, E.; Van Der Marel, G. A.; Codée, J. D. C.; Boot, R. G.; Davies, G. J.; Overkleeft, H. S.; Aerts, J. M. F. G. Detection of Active Mammalian GH31 α-Glucosidases in Health and Disease Using in-Class, Broad-Spectrum Activity-Based Probes. *ACS Cent. Sci.* **2016**, *2* (5), 351–358.

(13) Witte, M. D.; Kallemeijn, W. W.; Aten, J.; Li, K. Y.; Strijland, A.; Donker-Koopman, W. E.; Van Den Nieuwendijk, A. M. C. H.; Bleijlevens, B.; Kramer, G.; Florea, B. I.; Hooibrink, B.; Hollak, C. E. M.; Ottenhoff, R.; Boot, R. G.; Van Der Marel, G. A.; Overkleeft, H. S.; Aerts, J. M. F. G. Ultrasensitive in Situ Visualization of Active Glucocerebrosidase Molecules. *Nat. Chem. Biol.* **2010**, *6* (12), 907–913.

(14) Artola, M.; Wu, L.; Ferraz, M. J.; Kuo, C. L.; Raich, L.; Breen, I. Z.; Offen, W. A.; Codée, J. D. C.; Van Der Marel, G. A.; Rovira, C.; Aerts, J. M. F. G.; Davies, G. J.; Overkleeft, H. S. 1,6-Cyclophellitol Cyclosulfates: A New Class of Irreversible Glycosidase Inhibitor. *ACS Cent. Sci.* **2017**, *3* (7), 784–793.

(15) Wu, L.; Jiang, J.; Jin, Y.; Kallemeijn, W. W.; Kuo, C. L.; Artola, M.; Dai, W.; Van Elk, C.; Van Eijk, M.; Van Der Marel, G. A.; Codée, J. D. C.; Florea, B. I.; Aerts, J. M. F. G.; Overkleeft, H. S.; Davies, G. J. Activity-Based Probes for Functional Interrogation of Retaining β-Glucuronidases. *Nat. Chem. Biol.* **2017**, *13* (8), 867–873.

(16) Willems, L. I.; Beenakker, T. J. M.; Murray, B.; Scheij, S.; Kallemeijn, W. W.; Boot, R. G.; Verhoek, M.; Donker-Koopman, W. E.; Ferraz, M. J.; Van Rijssel, E. R.; Florea, B. I.; Codée, J. D. C.; Van Der Marel, G. A.; Aerts, J. M. F. G.; Overkleeft, H. S. Potent and Selective Activity-Based Probes for GH27 Human Retaining α-Galactosidases. *J. Am. Chem. Soc.* **2014**, *136* (33), 11622–11625.

(17) Marques, A. R. A.; Willems, L. I.; Herrera Moro, D.; Florea, B. I.; Scheij, S.; Ottenhoff, R.; van Roomen, C. P. A. A.; Verhoek, M.; Nelson, J. K.; Kallemeijn, W. W.; Biela-Banas, A.; Martin, O. R.; Cachón-González, M. B.; Kim, N. N.; Cox, T. M.; Boot, R. G.; Overkleeft, H. S.; Aerts, J. M. F. G. A Specific Activity-Based Probe to Monitor Family GH59 Galactosylceramidase, the Enzyme Deficient in Krabbe Disease. *ChemBioChem* **2017**, *18* (4), 402–412.

(18) Schröder, S. P.; De Boer, C.; McGregor, N. G. S.; Rowland, R. J.; Moroz, O.; Blagova, E.; Reijngoud, J.; Arentshorst, M.; Osborn, D.; Morant, M. D.; Abbate, E.; Stringer, M. A.; Krogh, K. B. R. M.; Raich, L.; Rovira, C.; Berrin, J. G.; Van Wezel, G. P.; Ram, A. F. J.; Florea, B. I.; Van Der Marel, G. A.; Codée, J. D. C.; Wilson, K. S.; Wu, L.; Davies, G. J.; Overkleeft, H. S. Dynamic and Functional Profiling of Xylan-Degrading Enzymes in Aspergillus Secretomes Using Activity-Based Probes. *ACS Cent. Sci.* **2019**, *5* (6), 1067–1078.

(19) Bezalel, L.; Shoham, Y.; Rosenberg, E. Characterization and Delignification Activity of a Thermostable α-l-Arabinofuranosidase from Bacillus Stearothermophilus. *Appl. Microbiol. Biotechnol.* **1993**, *40* (1), 57–62.

(20) Cartmell, A.; Muñoz-Muñoz, J.; Briggs, J. A.; Ndeh, D. A.; Lowe, E. C.; Baslé, A.; Terrapon, N.; Stott, K.; Heunis, T.; Gray, J.; Yu, L.; Dupree, P.; Fernandes, P. Z.; Shah, S.; Williams, S. J.; Labourel, A.; Trost, M.; Henrissat, B.; Gilbert, H. J. A Surface Endogalactanase in Bacteroides Thetaiotaomicron Confers Keystone Status for Arabinogalactan Degradation. *Nat. Microbiol.* **2018**, *3* (11), 1314–1326.

(21) Lopez, O. L.; Fernández-Bolaños, J. G.; Lillelund, V. H.; Bols, M. Aziridines as a Structural Motif to Conformational Restriction of Azasugars. *Org. Biomol. Chem.* **2003**, *1* (3), 478–482.

(22) Hövel, K.; Shallom, D.; Niefind, K.; Baasov, T.; Shoham, G.; Shoham, Y.; Schomburg, D. Crystallization and Preliminary X-Ray Analysis of a Family 51 Glycoside Hydrolase, the α-L-Arabinofuranosidase from Geobacillus Stearothermophilus T-6. *Acta Crystallogr. - Sect. D Biol. Crystallogr.* **2003**, *59* (5), 913–915.

(23) Tropea, J. E.; Cherry, S.; Waugh, D. S. Expression and Purification of Soluble His6-Tagged TEV Protease. *Methods Mol. Biol.* **2009**, *498*, 297–307.

(24) Gibson, D. G.; Young, L.; Chuang, R. Y.; Venter, J. C.; Hutchison, C. A.; Smith, H. O. Enzymatic Assembly of DNA Molecules up to Several Hundred Kilobases. *Nat. Methods* **2009**, *6* (5), 343–345.

(25) Wu, S.; Letchworth, G. J. High Efficiency Transformation by Electroporation of Pichia Pastoris Pretreated with Lithium Acetate and Dithiothreitol. *Biotechniques* **2004**, *36* (1), 152–154.

(26) Liu, W.; Tsou, C. lu. Determination of Rate Constant for the Irreversible Inhibition of Acetylcholine Esterase by Continuously Monitoring the Substrate Reaction in the Presence of the Inhibitor. *Biochim. Biophys. Acta (BBA)/Protein Struct. Mol.* **1986**, *870* (2), 185–190.

(27) Gray, P. J.; Duggleby, R. G. Analysis of Kinetic Data for Irreversible Enzyme Inhibition. *Biochem. J.* **1989**, *257* (2), 419–424.

(28) Miyanaga, A.; Koseki, T.; Matsuzawa, H.; Wakagi, T.; Shoun, H.; Fushinobu, S. Expression, Purification, Crystallization and Preliminary X-Ray Analysis of α-L-Arabinofuranosidase B from Aspergillus Kawachii. *Acta Crystallogr. Sect. D Biol. Crystallogr.* **2004**, *60* (7), 1286–1288.

(29) Winter, G.; McAuley, K. E. Automated Data Collection for Macromolecular Crystallography. *Methods* **2011**, *55* (1), 81–93.

(30) Vonrhein, C.; Flensburg, C.; Keller, P.; Sharff, A.; Smart, O.; Paciorek, W.; Womack, T.; Bricogne, G. Data Processing and Analysis with the AutoPROC Toolbox. *Acta Crystallogr. Sect. D Biol. Crystallogr.* **2011**, *67* (4), 293–302.

(31) Winter, G.; Lobley, C. M. C.; Prince, S. M. Decision Making in Xia2. *Acta Crystallogr. Sect. D Biol. Crystallogr.* **2013**, *69* (7), 1260–1273.

(32) Winn, M. D.; Ballard, C. C.; Cowtan, K. D.; Dodson, E. J.; Emsley, P.; Evans, P. R.; Keegan, R. M.; Krissinel, E. B.; Leslie, A. G. W.; McCoy, A.; McNicholas, S. J.; Murshudov, G. N.; Pannu, N. S.; Potterton, E. A.; Powell, H. R.; Read, R. J.; Vagin, A.; Wilson, K. S. Overview of the CCP4 Suite and Current Developments. *Acta*

Crystallogr. D. Biol. Crystallogr. **2011**, *67* (Pt 4), 235–242.

(33) McCoy, A. J.; Grosse-Kunstleve, R. W.; Adams, P. D.; Winn, M. D.; Storoni, L. C.; Read, R. J. Phaser Crystallographic Software. *J. Appl. Crystallogr.* **2007**, *40* (4), 658–674.

(34) Lebedev, A. A.; Young, P.; Isupov, M. N.; Moroz, O. V.; Vagin, A. A.; Murshudov, G. N. JLigand: A Graphical Tool for the CCP4 Template-Restraint Library. *Acta Crystallogr. Sect. D Biol. Crystallogr.* **2012**, *68* (4), 431–440.

(35) Emsley, P.; Lohkamp, B.; Scott, W. G.; Cowtan, K. Features and Development of Coot. *Acta Crystallogr. Sect. D Biol. Crystallogr.* **2010**, *66* (4), 486–501.

(36) Murshudov, G. N.; Skubák, P.; Lebedev, A. A.; Pannu, N. S.; Steiner, R. A.; Nicholls, R. A.; Winn, M. D.; Long, F.; Vagin, A. A. REFMAC5 for the Refinement of Macromolecular Crystal Structures. *Acta Crystallogr. Sect. D Biol. Crystallogr.* **2011**, *67* (4), 355–367.

(37) Car, R.; Parrinello, M. Unified Approach for Molecular Dynamics and Density-Functional Theory. *Phys. Rev. Lett.* **1985**, *55* (22), 2471–2474.

(38) Troullier, N.; Martins, J. L. Efficient Pseudopotentials for Plane-Wave Calculations. *Phys. Rev. B* **1991**, *43* (3), 1993–2006.

(39) Perdew, J. P.; Burke, K.; Ernzerhof, M. Generalized Gradient Approximation Made Simple. *Phys. Rev. Lett.* **1996**, *77* (18), 3865–3868.

(40) Marianski, M.; Supady, A.; Ingram, T.; Schneider, M.; Baldauf, C. Assessing the Accuracy of Across-the-Scale Methods for Predicting Carbohydrate Conformational Energies for the Examples of Glucose and α-Maltose. *J. Chem. Theory Comput.* **2016**, *12* (12), 6157–6168.

(41) Biarnés, X.; Ardèvol, A.; Planas, A.; Rovira, C.; Laio, A.; Parrinello, M. The Conformational Free Energy Landscape of β-D-Glucopyranose. Implications for Substrate Preactivation in β-Glucoside Hydrolases. *J. Am. Chem. Soc.* **2007**, *129* (35), 10686–10693.

(42) Ardèvol, A.; Rovira, C. Reaction Mechanisms in Carbohydrate-Active Enzymes: Glycoside Hydrolases and Glycosyltransferases. Insights from Ab Initio Quantum Mechanics/Molecular Mechanics Dynamic Simulations. *J. Am. Chem. Soc.* **2015**, *137* (24), 7528–7547.

(43) Laio, A.; Parrinello, M. Escaping Free-Energy Minima. *Proc. Natl. Acad. Sci. U. S. A.* **2002**, *99* (20), 12562–12566.

(44) Tribello, G. A.; Bonomi, M.; Branduardi, D.; Camilloni, C.; Bussi, G. PLUMED 2: New Feathers for an Old Bird. *Comput. Phys. Commun.* **2014**, *185* (2), 604–613.

(45) Huang, M.; Giese, T. J.; Lee, T. S.; York, D. M. Improvement of DNA and RNA Sugar Pucker Profiles from Semiempirical Quantum Methods. *J. Chem. Theory Comput.* **2014**, *10* (4), 1538–1545.

(46) Cremer, D.; Pople, J. A. A General Definition of Ring Puckering Coordinates. *J. Am. Chem. Soc.* **1975**, *97* (6), 1354–1358.

(47) Tiwary, P.; Parrinello, M. A Time-Independent Free Energy Estimator for Metadynamics. *J. Phys. Chem. B* **2015**, *119* (3), 736–742.

(48) Case, D. A.; Betz, R. M.; Cerutti, D. S.; Cheatham, T. E.; Darden, T.; Duke, R. E.; others. AMBER16, 2016. *San Fr.*

(49) Maier, J. A.; Martinez, C.; Kasavajhala, K.; Wickstrom, L.; Hauser, K. E.; Simmerling, C. Ff14SB: Improving the Accuracy of Protein Side Chain and Backbone Parameters from Ff99SB. *J. Chem. Theory Comput.* **2015**, *11* (8), 3696–3713.

(50) Wang, J.; Wolf, R. M.; Caldwell, J. W.; Kollman, P. A.; Case, D. A. Development and Testing of a General Amber Force Field. *J. Comput. Chem.* **2004**, *25* (9), 1157–1174.

(51) Jorgensen, W. L.; Chandrasekhar, J.; Madura, J. D.; Impey, R. W.; Klein, M. L. Comparison of Simple Potential Functions for Simulating Liquid Water. *J. Chem. Phys.* **1983**, *79* (2), 926–935.

(52) Miller, B. R.; McGee, T. D.; Swails, J. M.; Homeyer, N.; Gohlke, H.; Roitberg, A. E. MMPBSA.Py: An Efficient Program for End-State Free Energy Calculations. *J. Chem. Theory Comput.* **2012**, *8* (9), 3314–3321.

(53) Davies, G. J.; Planas, A.; Rovira, C. Conformational Analyses of the Reaction Coordinate of Glycosidases. *Acc. Chem. Res.* **2012**, *45* (2), 308–316.

(54) Speciale, G.; Thompson, A. J.; Davies, G. J.; Williams, S. J. Dissecting Conformational Contributions to Glycosidase Catalysis and Inhibition. *Curr. Opin. Struct. Biol.* **2014**, *28* (1), 1–13.

(55) Ardèvol, A.; Biarnés, X.; Planas, A.; Rovira, C. The Conformational Free-Energy Landscape of β-d-Mannopyranose: Evidence for a 1S5 → B2,5 → OS2 Catalytic Itinerary in β-Mannosidases. *J. Am. Chem. Soc.* **2010**, *132* (45), 16058–16065.

(56) Paës, G.; Skov, L. K.; O'Donohue, M. J.; Rémond, C.; Kastrup, J. S.; Gajhede, M.; Mirza, O. The Structure of the Complex between a Branched Pentasaccharide and Thermobacillus Xylanilyticus GH-51 Arabinofuranosidase Reveals Xylan-Binding Determinants and Induced Fit. *Biochemistry* **2008**, *47* (28), 7441–7451.

(57) Hövel, K.; Shallom, D.; Niefind, K.; Belakhov, V.; Shoham, G.; Baasov, T.; Shoham, Y.; Schomburg, D. Crystal Structure and Snapshots along the Reaction Pathway of a Family 51 α-L-Arabinofuranosidase. *EMBO J.* **2003**, *22* (19), 4922–4932.

(58) Van Rijssel, E. R.; Van Delft, P.; Lodder, G.; Overkleeft, H. S.; Van Der Marel, G. A.; Filippov, D. V.; Codée, J. D. C. Furanosyl Oxocarbenium Ion Stability and Stereoselectivity. *Angew. Chemie - Int. Ed.* **2014**, *53* (39), 10381–10385.

(59) Miyanaga, A.; Koseki, T.; Matsuzawa, H.; Wakagi, T.; Shoun, H.; Fushinobu, S. Crystal Structure of a Family 54 α-L-Arabinofuranosidase Reveals a Novel Carbohydrate-Binding Module That Can Bind Arabinose. *J. Biol. Chem.* **2004**, *279* (43), 44907–44914.

(60) Artola, M.; Wouters, S.; Schröder, S. P.; de Boer, C.; Chen, Y.; Petracca, R.; van den Nieuwendijk, A. M. C. H.; Aerts, J. M. F. G.; van der Marel, G. A.; Codée, J. D. C.; Overkleeft, H. S. Direct Stereoselective Aziridination of Cyclohexenols with 3-Amino-2-(Trifluoromethyl)Quinazolin-4(3H)-One in the Synthesis of Cyclitol Aziridine Glycosidase Inhibitors. *European J. Org. Chem.* **2019**, *2019* (6), 1397–1404.

(61) Jat, J. L.; Paudyal, M. P.; Gao, H.; Xu, Q. L.; Yousufuddin, M.; Devarajan, D.; Ess, D. H.; Ǩurti, L.; Falck, J. R. Direct Stereospecific Synthesis of Unprotected N-H and N-Me Aziridines from Olefins. *Science.* **2014**, *343* (6166), 61–65.

(62) Martens-Uzunova, E. S.; Schaap, P. J. Assessment of the Pectin Degrading Enzyme Network of Aspergillus Niger by Functional Genomics. *Fungal Genet. Biol.* **2009**, *46 Suppl 1* (1), S170–S179.

(63) Flipphi, M. J. A.; Visser, J.; van der Veen, P.; de Graaff, L. H. Cloning of the Aspergillus Niger Gene Encoding α-l-Arabinofuranosidase A.

Appl. Microbiol. Biotechnol. **1993**, *39* (3), 335–340.

(64) Flipphi, M. J. A.; van Heuvel, M.; van der Veen, P.; Visser, J.; de Graaff, L. H. Cloning and Characterization of the AbfB Gene Coding for the Major α-l-Arabinofuranosidase (ABF B) of Aspergillus Niger. *Curr. Genet.* **1993**, *24* (6), 525–532.

(65) Berrin, J. G.; Navarro, D.; Couturier, M.; Olivé, C.; Grisel, S.; Haon, M.; Taussac, S.; Lechat, C.; Courtecuisse, R.; Favel, A.; Coutinho, P. M.; Lesage-Meessen, L. Exploring the Natural Fungal Biodiversity of Tropical and Temperate Forests toward Improvement of Biomass Conversion. *Appl. Environ. Microbiol.* **2012**, *78* (18), 6483–6490.

(66) Schwarze, F. Wood Rotting Fungi: Fomes Fomentarius (L.: Fr.) Fr. Hoof or Tinder Fungus. *Top. Catal.* **1994**, *8* (1), 32–34.

(67) Zhou, S.; Raouche, S.; Grisel, S.; Navarro, D.; Sigoillot, J. C.; Herpoël-Gimbert, I. Solid-State Fermentation in Multi-Well Plates to Assess Pretreatment Efficiency of Rot Fungi on Lignocellulose Biomass. *Microb. Biotechnol.* **2015**, *8* (6), 940–949.

(68) Alexandropoulou, M.; Antonopoulou, G.; Fragkou, E.; Ntaikou, I.; Lyberatos, G. Fungal Pretreatment of Willow Sawdust and Its Combination with Alkaline Treatment for Enhancing Biogas Production. *J. Environ. Manage.* **2017**, *203*, 704–713.

SUPPLEMENTAL FIGURE AND TABLE CAPTIONS

Supplemental Figure 1. Inhibition kinetics of AnAbfA. A) Plot of rate vs. substrate concentration measured for AnAbfA hydrolyzing 4MU-Araf with the hyperbolic fit shown as a dotted line. B) Plot of fluorescence vs. time for AnAbfA in the presence of difference concentrations of inhibitor **1**. Each line represents the average of four measurements with the standard deviation represented as thinner lines above and below the average. C) Plot of fluorescence vs. time for AnAbfA in the presence of difference concentrations of inhibitor **6** as shown in panel B. D) Plot of apparent decay constant (k_{app}) extracted from an exponential decay fit of the curves shown in panel C vs. inhibitor concentration with the hyperbolic fit shown as a dotted line. Error bars are the standard deviation of the k_{app} values extracted from each of the four measured curves. Panels E and F are the same measurements as panels C and D, but made with inhibitor **2**. Panels G and H are the same measurements as panels C and D, but made with inhibitor **6**.

Supplemental Figure 2. Inhibition kinetics of AkAbfB. A) Plot of rate vs. substrate concentration measured for AkAbfB hydrolyzing 4MU-Araf with the hyperbolic fit shown as a dotted line. B) Plot of fluorescence vs. time for AkAbfB in the presence of difference concentrations of inhibitor **1**. Each line represents the average of four measurements with the standard deviation represented as thinner lines above and below the average. C) Plot of fluorescence vs. time for AkAbfB in the presence of difference concentrations of inhibitor **6** as shown in panel B. D) Plot of apparent decay constant (k_{app}) extracted from an exponential decay fit of the curves shown in panel C vs. inhibitor concentration with the hyperbolic fit shown as a dotted line. Error bars are the standard deviation of the k_{app} values extracted from each of the four measured curves. Panels E and F are the same measurements as panels C and D, but made with inhibitor **2**. Panels G and H are the same measurements as panels C and D, but made with inhibitor **6**.

Supplemental Figure 3: Determination of the impact of inner filter effects and stability of fluorescence over the course of the inhibition measurement. A) Epifluorescence intensity vs. [4MU] measured in 40 µL total volume of pH 7 phosphate buffer in a black 384-well plate using different excitation wavelengths. A linear best fit for F vs. [4MU] from 0.125 to 100 µM at 360 nm excitation is shown as a dashed blue line. A linear best fit for F vs. [4MU] from 0.125 to 500 µM at 390 nm excitation is shown as a dashed purple line. B) 4MU epifluorescence intensity measured over 200 minutes with a 15 second cycle time using an excitation wavelength of 360 nm at 25°C for concentrations ranging from 0.125-100 µM in 40 µL of pH 7 phosphate buffer in a black 384-well plate, plotted on a log scale.

Supplemental Figure 4: Comparison of inhibitor pre-treatment efficiency for blocking α-L-arabinofuranosidase active sites. To identify conditions suitable for blocking α-L-arabinofuranosidase active sites prior to probe labelling, pretreatments with 0.8-100 µM of inhibitors **1**, **2**, or **6** were performed followed by staining with probe **4**. Each pretreatment and staining was run in duplicate and were loaded into the gel in replicate pairs. The compound number and concentration are given above each pair of lanes.

Supplemental Figure 5. A) Crystals of GsGH51 grown at 293 K from a mixture of 1200 nL of 8 mg/mL GsGH51 in 5 mM Tris-HCl, 1 mM EDTA, pH 8 mixed with 600 nL of 0.1 M Tris-HCl, pH 7.5, 5% 2-propanol, 0.7 M NH_4F, 20% PEG3350. B) Crystals of EndoH-deglycosylated AkAbfB grown at 293 K from a mixture of 1200 nL of 10 mg/mL AkAbfB in 20 mM pH 5.0 sodium acetate mixed with 600 nL of 50% PEG400, 0.4 M Li_2SO_4, 100 mM sodium acetate, pH 4.5.

Supplemental Figure 6. Structure of the AkAbfB (E221Q) PNP-Araf Michaelis complex. A) Electron density of the PNP-Araf molecule (blue) within the AkAbfB (E221Q) active site (yellow) contoured to 1σ. Apparent hydrogen bonding interactions are shown as yellow dotted lines. B) Superposition of the AkAbfB (E221Q) Michaelis complex (yellow) with the AkAbfB product complex (fuchsia, PDBID: 1WD4).

Supplemental Figure 7. Deconvoluted intact MS measurements of GsGH51 before and after treatment with inhibitors **1** (A), **2** (B), and **6** (C). Predicted mass = 57406.3, expected Δm (**1**) = 146, expected Δm (**2**) = 145, expected Δm (**6**) = 226

Supplemental Figure 8. Deconvoluted intact MS measurements of AkAbfB before and after treatment with inhibitors **2** and **6**. The predicted mass is unknown due to unknown glycosylation remaining after EndoH treatment. Expected Δm (**2**) = 145, expected Δm (**6**) = 226. Note the additional peak series in the **6**-treated sample, which corresponds to a loss of 80 Da, the mass of SO_3. We attribute this to in-source fragmentation.

Supplemental Figure 9. Perturbation of the GsGH51 active site following reaction with inhibitor **2**. The complex with inhibitor **2** is shown in blue, the complex with inhibitor **6** is shown in cyan, and the complex with arabinofuranose (PDBID: 1PZ2) is shown in fuchsia. With the exception of Asn74 and Trp99 (shown for reference), the ligand and the active site residues with significantly different positions in complex with inhibitor **2** are shown as sticks.

Supplemental Figure 10. Overlay of PNP-Araf and inhibitor **2** in the active site of AkAbfB (E221Q) (gold) and AkAbfB (green), respectively, showing the displacement of the C1, C2, and O (or C6) positions between initial binding and the formation of the covalent intermediate.

Supplemental Figure 11. Fluorescence image (Cy5) following SDS-PAGE separation of *A. niger* arabinan secretome treated with ABP **4** in buffers at different pH values. A) Three separate gels, which were imaged in parallel, are shown, separated by black lines. The buffer used during treatment with ABP **4** is labelled above each lane (McI for McIlvane buffer and SPG for SPG buffer). B) Plot of normalized integrated band intensity vs. pH for both the upper (GH51) and lower (GH54) bands in the McI and SPG buffer systems.

Supplemental Figure 12. Simulated optimized Michaelis complex configurations of inhibitors **1** (A), **2** (B, C, D), and **6** (E) used for the calculation of binding energy within the active site of GsGH51. B shows the protonated general acid/base residue with deprotonated aziridine nitrogen, C shows the protonated general acid/base residue with protonated aziridine nitrogen, D shows the deprotonated general acid/base residue with protonated aziridine nitrogen.

Supplemental Figure 13. Simulated optimized Michaelis complex configurations of inhibitors **1** (A), **2** (B, C, D), and **6** (E) used for the calculation of binding energy within the active site of AkAbfB. B shows the protonated general acid/base residue with deprotonated aziridine nitrogen, C shows the protonated general acid/base residue with protonated aziridine nitrogen, D shows the deprotonated general acid/base residue with protonated aziridine nitrogen,

Supplemental Figure 14: Relative energies of the inhibitors binding to the active sites of GsGH51 and AkAbfB. Compounds **2**B, **2**C and **2**D corresponds to the different tested protonation states, following the labels used in Supplemental Figure 10 and 11. **2**B corresponds to protonated general acid/base with deprotonated aziridine nitrogen of **2**; **2**C corresponds to protonated general acid/base with protonated aziridine nitrogen of **2** and **2**D corresponds to deprotonated general acid/base with protonated aziridine nitrogen of **2**.

Supplemental Figure 15. A) Fluorescence image (Cy5) following SDS-PAGE separation of *A. niger* arabinan secretome treated with ABP **4** following incubation at different temperature values. The incubation temperature prior to labelling with ABP **4** is written above each lane in °C. B) and C) Replication of the experiment shown in A, but with the addition (B) or not (C) of 5 mM DTT prior to incubation at temperature. D) Plot of normalized integrated fluorescence intensity for the AbfA and AbfB bands vs. pre-treatment temperature. E) Plot of absolute integrated fluorescence intensity for the AbfA and AbfB bands across the same range of temperature with and without 5 mM DTT. The black line represents integrations from the gel in panel B and the red line represents integrations from the gel in panel C. F) Plot of initial 4MU-Araf hydrolysis rate vs. pre-incubation temperature for 5 µL of arabinan secretome diluted into 45 µL of 50 µM 4MU-Araf in pH 6.5 phosphate buffer. Each point represents the average of 4 technical replicates with error bars representing the standard deviation.

Supplemental Figure 16. SDS-PAGE of basidiomycete secretomes. A, B) Cy5 fluorescence scans of basidiomycete secretomes treated with ABP **4** and separated on SDS-PAGE. Labels are shown above each lane. L indicates ladder, A indicates secretome grown on aspen pulp, W indicates secretome grown on wheat straw, M indicates secretome grown on maltose, + indicates treatment with PNGaseF, - indicates no treatment with PNGaseF, the number above each lane is the BRFM number for the strain from which the secretome was isolated. C, D) Coomassie staining of the same gels shown in A and B; labelling is identical.

Supplemental Figure 17. Basidiomycete secretomes stained with ABP **4**. Panel A is white light imaging following Coomassie staining, panel C is Cy5 fluorescence, and panel B is Cy5 fluorescence (red) superimposed on the Coomassie image (image inverted, contrast optimized and false coloured green). Lane 1 contains 5 µL of Pageruler 10-180 kDa prestained ladder. Lanes 2-5 are *T. gibbosa, A. biennis, L. menziesii,* and *F. fomentarius,* respectively.

Supplemental Table 1: Kinetic parameters determined for the hydrolysis of 4MU-α-L-arabinofuranoside by AnAbfA and AkAbfB

Supplemental Table 2. Data collection and refinement statistics (molecular replacement).

Supplemental Table 3: Basidiomycete strains screened for α-L-arabinofuranosidase production.

FOR TOC ONLY